

1 **Elucidating the mechanisms of atmospheric new particle formation in the highly**
2 **polluted Po Valley, Italy**

3 Jing Cai¹, Juha Sulo¹, Yifang Gu¹, Sebastian Holm¹, Runlong Cai¹, Steven Thomas¹, Almuth Neuberger²,
4 Fredrik Mattsson², Marco Paglione³, Stefano Decesari³, Matteo Rinaldi³, Rujing Yin¹, Diego Aliaga¹, Wei
5 Huang¹, Yuanyuan Li^{1,4}, Yvette Gramlich², Giancarlo Ciarelli¹, Lauriane Quéléver¹, Nina Sarnela¹,
6 Katrianne Lehtipalo^{1,5}, Nora Zannoni³, Cheng Wu⁶, Wei Nie⁴, [Juha Kangasluoma¹](#), [Claudia Mohr^{7,8}](#),
7 Markku Kulmala^{1,4,9}, Qiaozhi Zha^{1,4}, Dominik Stolzenburg^{1,10*}, Federico Bianchi^{1*}

8 ¹ Institute for Atmospheric and Earth System Research, Faculty of Science, University of Helsinki, Helsinki
9 00014, Finland

10 ² Department of Environmental Science, Stockholm University, Stockholm 11418, Sweden

11 ³ Italian National Research Council-Institute of Atmospheric Sciences and Climate (CNR-ISAC), Bologna,
12 40129, Italy

13 ⁴ School of Atmospheric Sciences, Nanjing University, Nanjing, 210023, China

14 ⁵ Finnish Meteorological Institute, Helsinki, 00560, Finland

15 ⁶ Department of Chemistry and Molecular Biology, Atmospheric Science, University of Gothenburg,
16 Gothenburg 41296, Sweden

17 ⁷ Laboratory of Atmospheric Chemistry, Paul Scherrer Institute, Villigen, 5232, Switzerland

18 ⁸ Department of Environmental System Science, ETH Zurich, Villigen, 5232, Switzerland

19 ⁹ Beijing Advanced Innovation Center for Soft Matter Science and Engineering, Beijing University of
20 Chemical Technology, Beijing 100029, China

21 ¹⁰ Institute for Materials Chemistry, TU Wien, Vienna 1060, Austria

22 *Correspondence to:* federico.bianchi@helsinki.fi and dominik.stolzenburg@tuwien.ac.at

23 **Abstract**

24 New particle formation (NPF) is a major source of aerosol particles and cloud condensation nuclei in
25 the troposphere, playing an important role in both air quality and climate. Frequent NPF events have
26 been observed in heavily polluted urban environments, contributing to the aerosol number concentration
27 by a significant amount. The Po Valley region in northern Italy has been characterized as a hotspot for
28 high aerosol loadings and frequent NPF events in Southern Europe. However, the mechanisms of NPF
29 and growth in this region are not completely understood. In this study, we conducted a continuous 2-
30 month measurement campaign with state-of-the-art instruments to elucidate the NPF and the growth
31 mechanisms in Northern Italy. Our results demonstrate that in this area, frequent NPF events (66% of
32 all days during the measurement campaign) are primarily driven by abundant sulfuric acid ($8.5 \times 10^6 \text{ cm}^{-3}$)
33 and basic molecules. In contrast, oxygenated organic molecules from the atmospheric oxidation of

Formatted: Font: (Default) Times New Roman, 11 pt

34 volatile organic compounds (VOCs) appear to play a minor role in the initial cluster formation but
35 contribute significantly to the consecutive growth process. Regarding alkaline molecules, amines, are
36 insufficient to stabilize all sulfuric acid clusters in Po Valley. Ion cluster measurements and kinetic
37 models suggest that ammonia (10 ppb) must therefore also play a role in the nucleation process.
38 Generally, the high formation rates of sub-2 nm particles ($87 \text{ cm}^{-3} \text{ s}^{-1}$) and nucleation mode growth rates
39 (5.1 nm h^{-1}) together with the relatively low condensational sink ($8.9 \times 10^{-3} \text{ s}^{-1}$) will result in a high
40 survival probability of newly formed particles, making NPF crucial for the springtime aerosol number
41 budget. Our results also indicate that reducing key pollutants such as SO_2 , amine and NH_3 , could help
42 to decrease the particle number concentrations substantially in the Po Valley region.

43 1. Introduction

44 New particle formation (NPF) occurs ubiquitously in the troposphere and affects the global climate
45 (Dunne et al., 2016) and local or regional air quality (Kulmala et al., 2021). NPF and further growth of
46 the newly formed particles dominate aerosol number concentrations and are the major contributor to
47 the ultrafine (<100 nm) aerosol budget, which poses a significant health threat to the population in
48 polluted areas (Schraufnagel, 2020). While air pollution mitigation strategies mostly focus on reducing
49 particulate mass (particulate matter below $2.5 \mu\text{m}$ ($\text{PM}_{2.5}$)), ultrafine particle number concentrations
50 might not be affected by such policies (De Jesus et al., 2019). It is therefore essential that we understand
51 the mechanisms leading to NPF in polluted environments to design better targeted air quality strategies
52 for polluted European regions, where $\text{PM}_{2.5}$ reduction measures are already implemented.

53 NPF is closely linked to atmospheric air pollution. Efficient nucleation and growth are crucial factors
54 contributing to haze formation, according for over 65% of the particle number concentrations in urban
55 environment (Kulmala et al., 2021; Guo et al., 2014). Frequent NPF events have also been observed in
56 heavily polluted urban environments, including megacities in China (Chu et al., 2019; Yao et al., 2018;
57 Du et al., 2022), and India (Sebastian et al., 2022). Strong and frequent NPF events have been reported
58 in the most urbanization areas in China, such as the North China Plain (Wang et al., 2015; Wang et al.,
59 2013; Wu et al., 2011; Wu et al., 2007; Shen et al., 2011), Yangtze River Delta (Dai et al., 2017; Yu et
60 al., 2016; Xiao et al., 2015), and Peal River Delta (Yue et al., 2013; Peng et al., 2014; Liu et al., 2008).
61 This observation contradicts theoretical calculations that suggest NPF events are less likely to occur in
62 polluted areas, where high levels of preexisting aerosols acting as condensational sinks (CS) are capable
63 of quickly scavenging gaseous precursors of NPF (Kulmala et al., 2017).

64 The elucidation of NPF precursors and mechanisms has varied among different sampling locations and
65 studies. No uniform theory or mechanism can elucidate the NPF occurrence in different polluted areas
66 or in different seasons. For example, in Shanghai and Beijing, China, sulfuric acid (SA , H_2SO_4) and
67 amines were identified as key contributors to initial particle formations (Yao et al., 2018; Cai et al.,
68 2021; Yan et al., 2021). On the other hand, some studies also suggests that photooxidation products of
69 vehicle emitted organic vapors, dominate NPF in urban conditions rather than SA or base species (Guo
70 et al., 2020). Meanwhile, in Barcelona, Spain, which is significantly less polluted than Asian megacities
71 but still shows frequent high pollution levels, NPF was reported to be associated with SA along with
72 highly oxygenated organic molecules (HOMs) (Brean et al., 2020). The discrepancies in the reported
73 NPF mechanisms may arise from the limited utilization of state-of-the-art instruments, such as those
74 capable of measuring size distribution down to 1-2 nm and directly identifying clusters and vapors with
75 the influences by spatio-temporal variations (Wang et al., 2017). Therefore, gaining a better knowledge
76 of the key participants, nucleation mechanism and the roles of pre-existing particles is crucial for
77 comprehending the causes of the high NPF frequencies in polluted regions. This knowledge can be
78 essential for developing effective local $\text{PM}_{2.5}$ control and implementation strategies.

79 The Po Valley region is one of the most important industrial and agricultural areas in Southern Europe
80 with dense population (>17 million/ $70,000 \text{ km}^2$). It is located in northern Italy, surrounded by the Alps
81 (in the north), the Apennine mountains (in the south), and the Adriatic Sea (in the east). High primary
82 anthropogenic emissions, a mixture of numerous pollutants from industrial, urban and agricultural

Deleted: Our results show that abundant sulfuric acid, ammonia and amines from agricultural activities may be the dominant components driving the frequent NPF events (66% of all days during the measurement campaign) in this area. In contrast, oxygenated organic vapors seem to have a smaller role in cluster formation but contribute to the consecutive growth process. According to ion cluster measurements and kinetic model results, dimethylamine is not sufficient to stabilize all of the sulfuric acid during springtime in the Po Valley, suggesting that other amines and ammonia can also be involved. Generally, the high formation rates of sub-2 nm particles ($87 \text{ cm}^{-3} \text{ s}^{-1}$) and nucleation mode growth rates (5.1 nm h^{-1}) together with the relatively low condensational sink ($8.9 \times 10^{-3} \text{ s}^{-1}$) will result in a high survival probability of newly formed particles, making NPF crucial for the springtime aerosol number budget in the Po Valley region.

Formatted: Font: 11 pt

Formatted: Font: 11 pt

Formatted: Font: 11 pt

Formatted: Font: 11 pt

Formatted: Font: 11 pt

Formatted: Font: 11 pt

Formatted: Font: 11 pt

Formatted: Font: 11 pt

Formatted: Font: 11 pt

Formatted: Font: 11 pt

Formatted: Font: 11 pt

Formatted: Font: 11 pt

Formatted: Font: 11 pt

Formatted: Font: 11 pt

Formatted: Font: 11 pt

Formatted: Font: (Default) Times New Roman, 11 pt

Formatted: Font: (Default) Times New Roman, 11 pt

Formatted: Font: (Default) Times New Roman, 11 pt

Formatted: Font: (Default) Times New Roman, 11 pt

Formatted: Font: (Default) Times New Roman, 11 pt

Formatted: Font: (Default) Times New Roman, 11 pt

Formatted: Font: (Default) Times New Roman, 11 pt

Formatted: Font: (Default) Times New Roman, 11 pt

Formatted: Font: (Default) Times New Roman, 11 pt

Deleted: In theoretical calculations, it is generally assumed that NPF events are more favorable to occur in clean conditions due to lower concentrations of preexisting aerosols, which act as condensational sink (CS), capable of scavenging the gaseous precursors (Kulmala et al., 2017). However, frequent NPF events have also been observed in heavily polluted urban environments (Kulmala et al., 2017; Du et al., 2022), including megacities in China (Chu et al., 2019; Yao et al., 2018) and India (Sebastian et al., 2022). This phenomenon might be associated with the

136 sources, together with frequently occurring stagnant meteorological conditions in winter make the Po
137 Valley region a hotspot in Europe for high aerosol loadings (Saarikoski et al., 2012; Li et al., 2014;
138 Finzi and Tebaldi, 1982; Daellenbach et al., 2023), but distinct from Asian megacities as the population
139 density is significantly lower (250 people km⁻² in Po Valley compared to e.g., 1 400 people km⁻² in
140 Beijing), resulting in effects such as traffic or residential heating being less dominant pollution sources.
141 At the same time, NPF occurs frequently in the Po Valley (Hamed et al., 2007; Manninen et al., 2010).
142 For example, Shen et al. (2021) observed that NPF events took place on approximately 70% of the days
143 during spring and summer. Similarly, Kontkanen et al. (2017) discovered that during summer, NPF
144 occurred on 89% of the days. During NPF event days, high formation rates of sub-2nm neutral particles
145 (J_2 , $\sim 10^1$ to 10^2 cm⁻³ s⁻¹, (Kontkanen et al., 2017)) and SA concentrations ($\sim 1 \times 10^7$ cm⁻³) were observed
146 in the Po Valley (Paasonen et al., 2010; Kontkanen et al., 2017). These levels were among the highest
147 recorded in a study conducted at nine sites across the Northern Hemisphere (Kontkanen et al., 2017).

148 While previous studies conducted in the Po Valley have reported frequent NPF events characterized by
149 high nucleation and growth rates, the clustering mechanism and the dominant precursors for particle
150 growth have not been investigated to-date. Especially with respect to the distinct features of Po-Valley
151 compared to the more intensely researched megacity environments, a deeper understanding of frequent
152 NPF events, including their precursors, nucleation mechanisms, and growth processes is crucial for air
153 pollution control and the effective implementation of PM_{2.5} mitigation measures in such semi-urban but
154 highly industrialized regions as Po Valley. In this study, we conducted a 2-month field campaign in the
155 months of March – April 2022, we 1) identified the chemical composition of atmospheric neutral and
156 ion clusters by a set of state-of-the-art mass spectrometers, 2) characterized the initial NPF and further
157 growth rates using particle number size distribution measurement down to 1 nm, and 3) compared the
158 field measurement results with the recent Cosmics Leaving Outdoor Droplets (CLOUD) chamber
159 experiments to investigate the mechanism of NPF events in the Po Valley region. This allowed us to
160 elucidate the NPF and growth mechanisms at a severely polluted Southern European site, and to give
161 insights in best mitigation strategies for ultrafine particle pollution in the context of already
162 implemented PM_{2.5} reduction strategies.

163 2. Method

164 2.1 Measurement site

165 Our measurement was part of the Fog and Aerosol InterRAction Research Italy (FAIRARI) field
166 campaign in San Pietro Capofiume (SPC, 44.65°N, 11.62°E, 5 m a.s.l.), located in the Po Valley region
167 in Northern Italy. The measurement site is part of the Aerosol, Clouds and Trace Gases Research
168 Infrastructure (ACTRIS)-Italy network and operated by the Italian National Research Council-Institute
169 of Atmospheric Sciences and Climate (CNR-ISAC). The SPC site is approximately 30 km northeast of
170 Bologna (~400, 000 residents) and 20 km south of Ferrara (~130, 000 residents), the two major cities
171 in the area. The distance from the measurement site to the Adriatic Sea (to the east) is about 50 km. The
172 area around the sampling site consists of agricultural fields and a smaller town (<2, 000 inhabitants,
173 within 5 km) and smaller settlements in the proximity. Given its location, the SPC rural station is
174 considered to be representative of the regional background of the Po Valley (Paglione et al., 2021;
175 Paasonen et al., 2010; Hamed et al., 2007; Saarikoski et al., 2012; Decesari et al., 2014; Paglione et al.,
176 2020). The instruments for the NPF measurement were operated in a temperature controlled (~20 °C)
177 container from March 1 to April 30, 2022.

178 During the sampling period, the daily average temperature ranged from 1°C to 17°C. The average wind
179 speed (WS) was approximately 2.4 ± 1.5 m/s (Fig. 1b). The average WS in the daytime was 3.5 m/s from
180 the east, which was significantly higher than at night (1.5 m/s) from the west. Strong diurnal variations
181 of wind direction were observed, which was typically from the west at night and shifted to the east
182 during the day (Fig. 1a). This pattern was potentially influenced by the sea-land breeze from the Adriatic
183 Sea. Accordingly, the daily average relative humidity (RH) varied from 41% to 98%, with values as

Formatted: Font: (Default) Times New Roman, 11 pt

Formatted: Font: 11 pt

Formatted: Font: (Default) Times New Roman, 11 pt

Formatted: Font: (Default) Times New Roman, 11 pt, Superscript

Formatted: Font: (Default) Times New Roman, 11 pt

Formatted: Font: 11 pt

Deleted: make the Po Valley region a hotspot in Europe for high aerosol loadings (Saarikoski et al., 2012; Li et al., 2014; Finzi and Tebaldi, 1982; Daellenbach et al., 2023).

Formatted: Font: (Default) Times New Roman, 11 pt

Deleted: The aforementioned studies mainly characterized the NPF process in the Po Valley based on particle size distribution observations in terms of NPF frequency, nucleation and growth rates. Detailed knowledge on the mechanisms of NPF and further growth in the Po Valley is still limited. In this study, with

Formatted: Font: 11 pt

193 high as 85% at night, which sharply decreased to around 40% at noon caused by the strong temperature
194 variation.

195 2.2 Instruments

196 2.2.1 Chemical composition measurements

197 The chemical composition of cluster ions was measured using a high-resolution atmospheric-pressure-
198 interface time-of-flight mass spectrometer (APi-TOF, Aerodyne Research Inc. & ToFwerk AG). The
199 APi-TOF measures naturally charged ions present in the ambient environment. A detailed description
200 of the instrument can be found in Junninen et al. (2010). In this study, ambient air was sampled through
201 a 0.57-meter stainless steel tube with a flow rate of ~10 liters per minute (LPM), with 0.8 LPM of the
202 sample flow entering the APi-TOF.

203 The concentration of SA was measured using a nitrate ion (NO_3^-)-based chemical-ionization (CI)
204 atmospheric-pressure-interface time-of-flight mass spectrometer (CI-APi-TOF, Aerodyne Research Inc.
205 & ToFwerk AG (Jokinen et al., 2012)). The CI-APi-TOF is an APi-TOF coupled with a CI-unit,
206 equipped with a soft X-ray source (L9490, Hamamatsu's 9.5 kV) to produce the primary ions. The
207 sampling flow went into the instrument through a ~0.6-meter $\frac{3}{4}$ inch stainless steel tube. The sampling
208 flow was 10 LPM and the sheath flow was set to 20 LPM. Data acquisitions for CI-APi-TOF was
209 performed with a time resolution of 10 s. A calibration factor of $1.0 \times 10^{10} \text{ cm}^{-3}$ for SA was determined
210 with sampling loss corrections before the campaign according to the method proposed by Kurten et al.
211 (2012).

212 Dimethylamine (DMA) measurements were performed using a Vocus CI-ToF (time-of-flight) mass
213 spectrometer (hereafter Vocus, Aerodyne Research Inc. & ToFwerk AG) using H_3O^+ as a reagent ion.
214 The Vocus has been described in detail in Krechmer et al. (2018) and the study by Wang et al. (2020)
215 utilized Vocus for DMA observations. In this study, the Focusing Ion-Molecular Reactor (FIMR) of
216 Vocus operated at a pressure of 2.0 mbar and a temperature of 100 °C with the radio frequency
217 amplitude of 350 V and frequency of 1.4×10^6 Hz. Data acquisition was performed with a time
218 resolution of 10 s in the mass range 0–1000 amu.

219 2.2.2 Particle size distribution measurements

220 Particle Size Magnifier

221 The Airmodus A11 nano-CNC-system (nano-Condensation Nucleus Counter), colloquially known as
222 the Particle Size Magnifier (PSM) is a two-step condensation particle counter (CPC) capable of
223 measuring particle size distributions of sub-3nm particles (Vanhanen et al., 2011). The system consists
224 of two parts, in which the PSM (Airmodus A10) acts as a preconditioner where particles are grown first
225 before being funneled to the CPC (Airmodus A20) for further growth and optical detection. In the PSM
226 the sample flow is turbulently mixed with a heated flow saturated with diethylene glycol (DEG) in the
227 mixing section and the DEG then condenses on the particles in the growth tube. By scanning the flow
228 rate through the DEG saturator, the smallest activated particle size is altered which can be converted
229 into a sub-3nm particle size distribution. Further particle growth is achieved by butanol in the CPC such
230 that the particles reach optically detectable sizes.

231 The PSM was calibrated according to the standard operation procedure for PSM (Lehtipalo et al., 2022)
232 using a known aerosol population from a glowing tungsten wire generator (Kangasluoma et al., 2015;
233 Peineke et al., 2006). The detection efficiency for different particle sizes was determined by comparing
234 the concentration of size selected particles to a reference instrument, in this case a Faraday cup
235 electrometer (FEC).

236 The system was set up with an Airmodus Nanoparticle Diluter (AND) inlet (Lampimäki et al., 2023)
237 for sample dilution and automatic background measurement to make sure that the CPC stays within a
238 single counting range during the campaign. The inlet was set up at around 2 meters above the ground

239 and the background was measured roughly every 8 hours and subtracted from the signal during the
240 inversion process.

241 **HFDMPMS and Hauke-type DMPS**

242 The high-flow differential mobility particle sizer (HFDMPMS) system utilizes a half-mini differential
243 mobility analyzer (DMA_s (Fernández De La Mora and Kozłowski, 2013; Cai et al., 2018)) to size-select
244 particles that are then grown and detected by an A11 nano Condensation Nucleus Counter system
245 (Airmodus Ltd., A11 nano-CNC) (Kangasluoma et al., 2018). The **HFDMPMS** significantly improves
246 sub-10 nm particle measurements compared to a typical differential mobility particle sizer (DMPS)
247 system, allowing us to better characterize the sub-10 nm particle size distribution when combined with
248 the PSM measurements. The **DMA** was size-calibrated with electro sprayed positively charged
249 monomer ions of tetraheptylammonium bromide (THA⁺) (Ude and De La Mora, 2005).

Formatted: Highlight

Deleted: A11 nano-CNC system

250 The HFDMPMS inlet was set up at a height of 1 m and used a 50 cm long 10 mm outer diameter tube
251 with a core sampling system to minimize losses (Kangasluoma et al., 2016; Fu et al., 2019). A home-
252 built Soft X-Ray ionization source (similar to the TSI Inc. Model 3087) was used to charge particles.
253 The **HFDMPMS** measured the particle size-distribution from 2–15 nm for both polarities at 15 predefined
254 size-steps within 10 minutes.

Formatted: Highlight

Deleted: (Fernández De La Mora and Kozłowski, 2013).

255 Sampling from the same inlet and using the same charging device, a conventional DMPS system
256 equipped with a Hauke-type DMA (aerosol flow 1 LPM, sheath flow 5 LPM) and a TSI Inc. CPC
257 (Model 3772) was measuring the particle size-distribution from 10–800 nm at 16 predefined size-steps
258 within 10 minutes. In addition, a DMPS measuring from 15–800 nm was available in another
259 measurement container at the same field site. The total particle number concentrations measured
260 routinely with the CPCs after a size-scanning cycle of each DMPS system was compared with a
261 reference CPC (TSI Inc. Model 3025A) operated at the same site during the first weeks of the campaign.
262 It revealed on average a factor of 2 lower concentrations measured by the **Hauke-type DMPS** which
263 was confirmed to be rather size-independent by a comparison of the measured size-distributions and
264 their overlap with the **Halfmini**-DMPS system and was thus subsequently corrected for.

Formatted: Highlight

Formatted: Highlight

265 **2.2.3 Co-located measurements**

266 Additional co-located measurements of auxiliary data from CNR-ISAC network (www.isac.cnr.it/en)
267 and from the routine monitoring program of the Regional environmental protection agency of Emilia
268 Romagna (ARPAE, <https://www.arpae.it/it>) were used in this study. [An online High-Resolution Time-](#)
269 [of-Flight Aerosol Mass Spectrometer \(HR-ToF-AMS, Aerodyne Research\) and a Multi Angle](#)
270 [Absorption Photometer \(MAAP, Thermo Scientific\) were operated on the same site for the](#)
271 [measurement of non-refractory species and black carbon \(BC\), respectively.](#) Trace gases were also
272 measured with 1 minute time resolution: O₃ (Thermo Scientific, model TEI-49i), NO_x (Teledyne-API,
273 model 200A), NH₃ (Teledyne-API, model 201E), and SO₂ (Thermo Scientific, Model 43i Trace Level-
274 Enhanced). Moreover, meteorological parameters (e.g., RH, temperature, wind direction and wind
275 speed) were measured by a meteorology station (VAISALA Ltd, model wxt536).

276

277 **2.3 Data processing**

278 **2.3.1 New particle formation classification**

279 We classified each day according to whether a growing mode appeared in the particle size distribution
280 or not. This classification was done separately for both the **HFDMPMS** and the PSM size distributions. A
281 growing mode was defined as a new particle mode that appeared in the particle size distribution and
282 continued to grow to larger sizes for at least two hours. If there was a growing mode visible in both the
283 PSM and **HFDMPMS** size distributions, the day was defined as "NPF with growth". If there was no
284 growth or the growth was unclear in the **HFDMPMS** size distribution but there was a growing mode in
285 the PSM size distribution, then the day was classified as "NPF with no growth". If there was no growing
286 mode in either size distribution, then the day was marked as "no NPF events". The definition is similar
287 to Dada et al. (2018) who used naturally charged ions to separate between NPF days with clustering

Formatted: Highlight

Formatted: Highlight

Formatted: Highlight

334 observed new particle formation without growth (Fig. S1). In total we observed new sub-3 nm clusters
335 forming on 66 % of the days. Even though we applied the similar definition of NPF events as previous
336 study, we can only compare our NPF events with growth type with the reported NPF event frequency
337 due to the lack of capacity to measure the sub-3nm particles in previous literature. Our results were
338 similar to those by Hamed et al. (2007) who observed NPF events on 36 % of the time in March and
339 April of 2002 at the same site. Manninen et al. (2010) observed NPF events during more than half of
340 all days from March to Oct in 2008 and Kontkanen et al. (2016) observed NPF during 89 % of the days
341 in July at the same site, which is higher than our observations. Hamed et al. (2007) also observed that
342 NPF with growth events on 60% of the days during summer, which suggests that summertime NPF
343 frequency at SPC is typically higher than our observation in springtime 2022. This difference in the
344 observed NPF frequency was likely due to the different season with favorable conditions for NPF such
345 as potential lower CS (due to less stagnant meteorological conditions) and higher basic and organic
346 molecule concentrations in summer. In addition, the abundant solar radiation and low aerosol water
347 content (limiting surface area and heterogenous reactions (Du et al., 2022)), likely create favorable
348 conditions for NPF to occur.

349 The median average particle formation rates at 1.7 nm, 3 nm and 7 nm for all sampling days with NPF
350 with growth events were $87 \text{ cm}^{-3} \text{ s}^{-1}$ ($32 - 133 \text{ cm}^{-3} \text{ s}^{-1}$), $3.2 \text{ cm}^{-3} \text{ s}^{-1}$ ($1.4 \text{ cm}^{-3} \text{ s}^{-1} - 7.0 \text{ cm}^{-3} \text{ s}^{-1}$) and 1.4
351 $\text{cm}^{-3} \text{ s}^{-1}$ ($0.3 \text{ cm}^{-3} \text{ s}^{-1} - 3.0 \text{ cm}^{-3} \text{ s}^{-1}$), respectively. The formation rate at 1.7 nm during NPF with growth
352 days (NPF with growth, $87 \text{ cm}^{-3} \text{ s}^{-1}$) is similar to that observed previously at the same site by Kontkanen
353 et al. (2016) in summer. The high formation rate, which is comparable with heavily polluted urban
354 environments such as Beijing and Shanghai, China ($59 \text{ cm}^{-3} \text{ s}^{-1} - 225 \text{ cm}^{-3} \text{ s}^{-1}$ (Deng et al., 2020; Yao
355 et al., 2018)), will be further discussed in section 3.4. The average formation rate ($J_{1.7}$) on NPF days
356 without growth ($24 \text{ cm}^{-3} \text{ s}^{-1}$) is much lower. During the noontime, the formation rate of particles for
357 NPF events with no growth was less than half of $J_{1.7}$ for NPF with growth (Fig. S2). It suggests that for
358 particles to grow in a polluted environment such as the Po Valley, there needs to be abundant clustering
359 to overcome losses to the existing condensation sink so that at least some of the particles survive to
360 grow into larger sizes.

361 SA has long been known as a primary gaseous precursor for NPF in continental environments, owing
362 to its extremely low volatility (Kirkby et al., 2011; Kulmala et al., 2013). During our sampling period,
363 we observed high SA concentration in the Po Valley, in accordance with the frequent NPF events. The
364 daily average SA concentration measured between 10:00 – 14:00 LT was $4.6 \times 10^6 \text{ cm}^{-3}$, which increased
365 to $8.5 \times 10^6 \text{ cm}^{-3}$ during NPF events with growth, aligning with previous findings from the same site
366 ($1.6 \times 10^7 \text{ cm}^{-3}$ during NPF in summer of 2009, (Paasonen et al., 2010)). Over the entire sampling period
367 (10:00 – 14:00 LT), SA showed a moderately correlation with the calculated $J_{1.7}$ ($r = 0.49$, Spearman
368 correlation coefficient, for the logarithmic values), but its relationship varied among different days. This
369 suggests that in addition to SA, other components, such as basic molecules, may also contribute to
370 driving NPF events and subsequent growth in the Po Valley.” ▲

371 3.2 Nucleation mechanism

372 To investigate the NPF mechanism in the Po Valley, in this study we firstly compared the
373 simultaneously measured $J_{1.7}$ and SA with recent Cosmics Leaving Outdoor Droplets (CLOUD)
374 chamber experiments that simulated NPF under polluted boundary layer conditions with anthropogenic
375 emissions (Xiao et al., 2021). In those experiments, amines, ammonia, as well as aromatics were added
376 to reflect a heavily anthropogenic emission-influenced environment. Certain basic molecules, including
377 amines (e.g., dimethylamine (DMA)) and ammonia (NH_3) have been shown to substantially enhance
378 nucleation and reduce evaporation by stabilizing atmospheric SA in chamber studies (Almeida et al.,
379 2013). Besides, OOMs can also contribute to NPF and subsequent particle growth, even without the
380 inclusion of SA (Kirkby et al., 2016; Xiao et al., 2021). As shown in Fig. 3a, most of the measurements
381 were above the SA- NH_3 system at 278K from the CLOUD chamber, suggesting the SA- NH_3 mechanism
382 itself cannot solely explain the measured $J_{1.7}$ and that other species are most likely participating to NPF

Deleted: higher boundary layer mixing and

Moved (insertion) [1]: Previous studies have demonstrated that SA is the most important gaseous precursor for NPF in continental environments due to its extremely low volatility (Kirkby et al., 2011; Kulmala et al., 2013). During the sampling period, high SA concentration was measured in the Po Valley, concurrent with the frequent NPF events. The daily average concentration of SA was $4.6 \times 10^6 \text{ cm}^{-3}$ (10:00 – 14:00 LT), similar to those in polluted megacities in China ($5 \times 10^6 \text{ cm}^{-3} - 7 \times 10^6 \text{ cm}^{-3}$). During the NPF with growth days, the SA concentration was as high as $8.5 \times 10^6 \text{ cm}^{-3}$. The generally high concentrations were consistent with a previous study conducted at the same site ($1.6 \times 10^7 \text{ cm}^{-3}$ during NPF in summer of 2009, (Paasonen et al., 2010)). For the entire sampling period, SA was moderately correlated with the calculated $J_{1.7}$ ($r = 0.49$, Spearman correlation coefficient, for the logarithmic values) but varied among different days. This suggests that in addition to SA, other components, such as basic molecules and oxygenated organic molecules (OOMs), may also play a crucial role in driving NPF events and further growth in the Po Valley. ¶

Deleted: Previous studies have demonstrated that SA is the most important gaseous precursor for NPF in continental environments due to its extremely low volatility (Kirkby et al., 2011; Kulmala et al., 2013). During the sampling period, high SA concentration was measured in the Po Valley, concurrent with the frequent NPF events. The daily average concentration of SA was $4.6 \times 10^6 \text{ cm}^{-3}$ (10:00 – 14:00 LT), similar to those in polluted megacities in China ($5 \times 10^6 \text{ cm}^{-3} - 7 \times 10^6 \text{ cm}^{-3}$). During the NPF with growth days, the SA concentration was as high as $8.5 \times 10^6 \text{ cm}^{-3}$. The generally high concentrations were consistent with a previous study conducted at the same site ($1.6 \times 10^7 \text{ cm}^{-3}$ during NPF in summer of 2009, (Paasonen et al., 2010)). For the entire sampling period, SA was moderately correlated with the calculated $J_{1.7}$ ($r = 0.49$, Spearman correlation coefficient, for the logarithmic values) but varied among different days. This suggests that in addition to SA, other components, such as basic molecules and oxygenated organic molecules (OOMs), may also play a crucial role in driving NPF events and further growth in the Po Valley. ¶

Formatted: Font: (Default) Times New Roman, 11 pt

Formatted: Font: 11 pt, Bold

Moved up [1]

428 in the Po Valley. For instance, amines, such as DMA or TMA, with higher basicity may contribute to
429 NPF, consistent with not negligible concentrations of amines in previous studies in the aerosol at SPC
430 (Paglione et al., 2014; Decesari et al., 2014). For the whole sampling period, the median SA and $J_{1,7}$
431 values in Po Valley follows the SA-DMA-NH₃ (4 ppt DMA and 1ppb NH₃) and SA-DMA-NH₃-Org
432 (adding additional oxidized aromatic organics (Xiao et al., 2021)) lines from the CLOUD chamber at
433 293K even though during most of the NPF days the average noontime temperature was around 285K
434 (Fig. 3a).

435 The SA dimer measured by CI-API-TOF is typically used as an indicator for the initial step for the
436 cluster formation in NPF events (Yan et al., 2021). According to a previous study (Yan et al., 2021),
437 the source and sink terms of the SA dimer can be determined by calculating the formation rate from SA
438 monomer collisions and the loss rate from the SA dimer through coagulation onto pre-existing particles
439 (Fig. 2b). In general, the correlation coefficient between SA dimer and its source to sink term ratios (r
440 = 0.80, Spearman correlation coefficient) indicated that similar to Chinese urban areas, SA dimer was
441 in a pseudo steady-state between the formation of SA monomer collision and the loss onto CS by
442 coagulation.

443 To further assess the influence of DMA, one of the most common and efficient base molecules for NPF
444 in urban environments (Yao et al., 2018), we compared the measured SA dimer concentrations with the
445 simulated ones under different DMA levels (from 0.1 ppt to reaching kinetic limit) by the kinetic model
446 (Fig. 3b). From our cluster kinetics simulations, during the peak hours of NPF, DMA concentrations
447 are expected to be in the range of 0.1 ppt to 5 ppt, which is lower than the need for reaching the kinetic
448 limit (Figs. 3b and S3). It implies that other factors, for example, the abundant ambient NH₃
449 concentrations (~10 ppb) or trimethylamine (TMA) during our study period may also participate in
450 cluster formation. It is consistent with the Vocus measurement, which suggests the ambient DMA
451 signals were close to the background levels (Fig. S4). The reason for not reaching SA-DMA limit during
452 the campaign could be 1) the relatively lower DMA emissions (such as vehicle flows) than Chinese
453 megacities (Ge et al., 2011; Zhu et al., 2022), and 2) the quickly scavenge caused by photolysis and
454 nighttime high RH (85%) (Leng et al., 2015; Yao et al., 2016). Therefore, both of the abundant ambient
455 NH₃ concentrations (~10 ppb) and amines likely participated in cluster formation during our study
456 period.

457 Median particle growth rates (GR) during NPF events for 1.5 – 3 nm, 3 – 7 nm, 7 – 15 nm were 1.3
458 (1.0– 2.4) nm h⁻¹, 4.6 (2.9 – 5.8) nm h⁻¹, and 5.1 (3.8 – 8.8) nm h⁻¹, respectively. The values in brackets
459 represent the 25th and the 75th percentile of data (Fig. 3c). Growth rates increase with particle diameters,
460 a phenomenon observed in other campaigns around the world as well (Kontkanen et al., 2017, Kulmala
461 et al., 2013)) typically indicative of an increasing organic vapors contribution with size (e.g.,
462 Stolzenburg et al. (2018)). The growth rates observed here were similar to those observed by Kontkanen
463 et al. (2016) at SPC in summer (7.2 nm h⁻¹ for 7 – 20 nm) and our 1.5 – 3 nm growth rate matches well
464 with Manninen et al. (2010) (1.5 nm h⁻¹) during spring in the Po Valley. A comparison to predicted
465 growth rates from sulfuric acid condensation without organics, which was calculated based on kinetic
466 collisions of the measured SA concentrations and the effect of van-der-Waals forces on the collision
467 frequency ((Stolzenburg et al., 2020), Fig. 3c), suggests that sulfuric acid condensation may be on
468 average sufficient for the growth of the smallest clusters (below 3 nm). It supports the argument that in
469 the initial steps of NPF and growth in Po Valley sulfuric acid and its stabilizing molecules (likely the
470 bases NH₃ and amines) were controlling particle formation. However, for particles to grow beyond 3
471 nm in size other vapors were needed, which was suggested by the significantly lower contribution of
472 growth by SA (indicated by the green line) than the measured GR for 3 – 7 nm and 7 – 15 nm (Fig. 3c).
473 Those vapors were likely a mixture of organics of anthropogenic and biogenic origin (with the latter
474 emitted at higher rates during summer, which could cause the slightly higher values in Kontkanen et al.
475 (2017)). We compared the GR during NPF with and without growth events using the method proposed
476 in Kulmala et al. (2022) where the signal was averaged for all classified non-event days and then an

Formatted: Font: 11 pt

Deleted: even though it was difficult to quantify during the campaign due to the absence of a suitable calibration method. The reason for not reaching SA-DMA limit during the campaign could be 1) the relatively low emissions such as vehicle flows near our sampling site that are reported to be the main sources for DMA in Chinese urban areas (Ge et al., 2011; Zhu et al., 2022), 2) the nighttime high RH (85%) and daytime photolysis process quickly scavenge gaseous DMA by wet deposition, heterogeneous reaction and photolysis (Leng et al., 2015; Yao et al., 2016).

487 appearance time fit was performed for each size channel independently, revealing also a growth pattern.
488 We found no significant difference for the GR in 7 – 15 nm size range (GR=5.1 nm h⁻¹ in NPF with
489 growth days and average GR=6.1 nm h⁻¹ in NPF without growth days). Considering the similar CS and
490 GR levels for NPF with and without growth days, the higher formation rates at 1.7 nm (87 cm⁻³ s⁻¹) may
491 be a more important factor to surpass the CS. In stable meteorological conditions, a higher formation
492 rate may significantly elevate the possibility of newly formed particles overcome the CS and continuous
493 grow to larger sizes.

Formatted: Font: 11 pt

Deleted: Considering the similar CS and GR levels for NPF with and without growth days, the higher formation rates at 1.7 nm (87 cm⁻³ s⁻¹) may be the decisive factor to overcome the CS and determine if a growing mode can be observed leading to a classification of the day as an NPF with growth day.

3.3 Ion and neutral clusters and further particle growth

494 During the campaign, we observed and identified different types of ion clusters with cluster ion
495 measurements using the APi-TOF, including SA-NH₃, SA-Amine, SA-NH₃-Amine, SA-NH₃-Org
496 during NPF. In Fig. 4a, we presented the mass defect plot of the naturally charged ion clusters on April
497 20th, when strong NPF events were observed ($J_{1.7}$: 83 cm⁻³ s⁻¹). The presence of these clusters was
498 usually in conjunction with SA tetramers (SA₄), pentamers (SA₅), and hexamers (SA₆), which
499 potentially contribute to the NPF events. In Api-TOF measurement, the absence of basic species in the
500 smallest sulfuric acid clusters is likely attributed to the loss of base molecules within the mass
501 spectrometer (Cai et al., 2022b; Zha et al., 2023; Alfaouri et al., 2022).

Formatted: Font: 11 pt

Deleted: Acid-base clusters were not observed in monomer (SA₁), dimer (SA₂), or trimers (SA₃), likely due to declustering effects in the APi-TOF instrument (Cai et al., 2022b; Zha et al., 2023; Alfaouri et al., 2022).

Deleted: escape

Deleted: B

503 Among all SA-base (SA-B) clusters, the most abundant SA-NH₃ clusters were from SA₄-B to SA₆-B
504 (Fig. 4a), even though they are reported to be more easily evaporated than DMA clusters due to
505 collision-induced dissociation (Passananti et al., 2019). Pure SA-Amine clusters were only found in the
506 SA₄-B clusters with different types of amines, including methylamine (C₁-amine), DMA (C₂-amine),
507 trimethylamine (C₃-amine), and butylamine (C₄-amine). The detection of other SA-B than SA-DMA
508 clusters indicates that other candidate bases could also play a crucial role in the complex atmosphere
509 for nucleation. For example, a recent study conducted in Beijing highlights the importance of TMA,
510 which can enhance nucleation rate from SA-DMA system by 50% – 100% (Cai et al., 2023b). In the Po
511 Valley, the signal intensity of SA₄-NH₃ was significantly higher than that of the pure SA₄-amine clusters
512 (~2 times) even though amines (e.g., DMA) were proven to be more efficient (~3 orders of magnitude)
513 than NH₃ in clustering (Almeida et al., 2013). SA-NH₃-Amine clusters could be found along with SA-
514 NH₃ clusters in SA₅-B and SA₆-B. Similar patterns of the high fractions of SA-NH₃ and SA-NH₃-
515 Amine clusters were also reported in the CLOUD chamber studies under relatively low DMA and high
516 NH₃ conditions (Schobesberger et al., 2013). Therefore, it can be concluded that a large amount of NH₃
517 also participates in NPF in the Po Valley region. Meanwhile, with a much lower amount, amines may
518 also play a crucial role in the formation of small clusters (SA₄-B) due to their high stabilization
519 efficiencies.

Deleted: that

Deleted: accelerate

Deleted: the

Deleted: formation

Deleted: It is different from Chinese cities such as Shanghai (Yao et al., 2018), where high signals of SA₄-DMA clusters were found even with CI-API-TOF which is more easy for declustering.†

520 Moreover, some SA-NH₃-Org and I-containing ion clusters were also observed on NPF days, but to a
521 much lower extent than clusters involving NH₃ or DMA. It has been shown in previous CLOUD
522 chamber studies that the oxidation products of anthropogenic volatile organic compounds (AVOCs, e.g.,
523 naphthalene, trimethylbenzene and toluene) can largely promote the formation rate of particles (Xiao
524 et al., 2021). The I-containing ions (mainly IO₃⁻) likely originated from the Adriatic Sea during the
525 daytime, which was indicated by the easterly wind. Since no large iodine clusters were identified in the
526 APi-TOF (e.g., (HIO₃)₀₋₁(I₂O₅)_n·IO₃⁻, (He et al., 2021)), iodine-induced new particle formation in the
527 Po Valley may not be as important as the pristine marine environment (Sipila et al., 2016). During NPF
528 without growth days, the formation mechanism was similar to the NPF days regarding the ion cluster
529 measurement (Fig. S5).

530 The SA monomer in the Po Valley can be observed during the peak hours (10:00 – 14:00 LT) in both
531 NPF and non-NPF days, but much lower SA dimer or trimers were found in the non-NPF days (Figs.
532 4b, and S6). In the nighttime, the SA concentrations were close to zero due to the scavenging of SO₂
533 and SA by hydrated aerosol and hygroscopic growth of particles, as indicated by the high RH (Fig. 1).
534 During our sampling period, large amounts of organics were identified by the CI-API-TOF. They were

Deleted: Similar to polluted cities such as Beijing or Shanghai, the

Formatted: Subscript

Deleted: effect of

558 typically smaller than 400 Th with carbon numbers < 8 and oxygen numbers < 6 (Fig. S7). Due to the
559 relatively high NO_x levels (13 ppb) that can terminate the dimerization reactions (Yan et al., 2020), no
560 OOM dimers were found, which is different from clean and biogenically dominated environments such
561 as Hyytiälä (Lehtipalo et al., 2018). The compositions of OOMs were similar between NPF and non-
562 NPF days but with different abundance. Extremely high abundances of nitrophenols and their
563 homologous compounds were found on non-NPF days (~8 times higher than on NPF days), likely
564 caused by both of the enhanced primary (e.g., biomass burning (Mohr et al., 2013) and pesticide usage
565 (Harrison et al., 2005)) and secondary (e.g., photochemical and/or aqueous-phase secondary formation)
566 sources (Zheng et al., 2021; Gilardoni et al., 2016). C₂₋₄H₄₋₅N₀₋₁O₃₋₄ compounds were found to be 50%
567 higher (Fig. S7) on non-NPF days due to the higher RH and the enhanced heterogeneous reactions that
568 form smaller organics such as carboxylic acids. Previous studies also reported aqueous-phase organic
569 aerosol processing at high RH (Gilardoni et al., 2016) and high concentrations of carboxylic acids such
570 as formic, oxalic, and malonic acids in the springtime in the Po Valley (Saarikoski et al., 2012). In
571 general, the fraction of the abundance of nitrogen-containing OOMs (CHON) of total identified OOMs
572 were 60% – 70%, which is close to the levels reported in polluted cities such as Nanjing (Nie et al.,
573 2022) and Beijing (Guo et al., 2022). A slightly higher fraction of CHON compounds (73 %) was found
574 during non-NPF days than NPF days (67 %), consistent with higher NO_x and fine particulate matter
575 levels (Fig. S8). It is likely associated with the stagnant meteorological conditions and accumulation of
576 pollutants during the non-NPF days. However, the overall high amounts of CHON compounds and the
577 lack of organic dimers make it unlikely that OOMs drive the NPF process in the sub-3nm range (both
578 clustering and initial growth, see e.g., Simon et al. (2020)). Their similar abundance on non-NPF and
579 NPF days was also in line with the similar estimated GR for both types of days.

580 Throughout the entire sampling period, relatively high concentrations of fine particulate matters (PM_{2.5})
581 were measured, with a daily average of 17 μg m⁻³ and a maximum value of 43 μg m⁻³. Correspondingly,
582 the hourly CS levels, which quantify the ability of pre-existing particles to scavenge gaseous precursors,
583 ranged from <1×10⁻⁴ s⁻¹ to 3×10⁻² s⁻¹ with an average value of 5.4×10⁻³ s⁻¹. Previous studies in polluted
584 areas, such as Chinese megacities, have shown that NPF events are closely linked to CS levels (Cai et
585 al., 2017). NPF probability was reported to decreased to 50% when CS was around 1×10⁻² s⁻¹ and
586 completely shut off with CS of 6×10⁻² s⁻¹ (Du et al., 2022). However, in the Po Valley, we observed no
587 strong influence of CS on NPF events, with only a slightly difference in CS during the noontime of non-
588 NPF days (median: 9.4×10⁻³ s⁻¹) than NPF days (median: 8.6×10⁻³ s⁻¹).

Deleted: during the non-NPF days

Deleted: as no organic molecules of extremely- or ultra-low volatility were formed

Formatted: Font: 11 pt

Formatted: Font: 11 pt

Formatted: Font: 11 pt

Formatted: Font: 11 pt

Formatted: Font: 11 pt

Deleted: ¶

Formatted: Font: (Default) +Body (Calibri)

593 3.4 Comparison between Po Valley and other environments

594
595 Even though the measured $J_{1,7}$ in Po Valley was at the same level of the values found in Chinese polluted
596 megacities, it was much higher than in clean environments, such as the boreal forest of Hyytiälä in
597 Finland, mountain sites Jungfrauoch in Switzerland, and Chacaltaya in Bolivia ($1.5 \text{ cm}^{-3} \text{ s}^{-1}$ – 2.0 cm^{-3}
598 s^{-1} , Fig. 5a). The average SA concentrations ($4.6 \times 10^6 \text{ cm}^{-3}$, 10:00 – 14:00 LT) were comparable to the
599 levels observed in polluted megacities in China (ranging from $3.9 \times 10^6 \text{ cm}^{-3}$ to $7.4 \times 10^6 \text{ cm}^{-3}$, Fig. 5c),
600 but significantly higher than those in remote areas like Hyytiälä ($9 \times 10^5 \text{ cm}^{-3}$) and the Jungfrauoch
601 ($5 \times 10^5 \text{ cm}^{-3}$)... SA concentrations during NPF days ($8.6 \times 10^6 \text{ cm}^{-3}$) in the Po Valley were twice as high
602 as those on non-NPF days ($4 \times 10^6 \text{ cm}^{-3}$). This difference may be linked to the significant variations (t-
603 test, $p < 0.05$) of SO_2 concentrations between NPF days (0.38 ppbv) and non-NPF days (0.20 ppbv). This
604 contrasts with findings in Beijing, where similar or even higher levels of SA and SO_2 were observed
605 during non-NPF days compared to NPF event days (Yan et al., 2021). The variations in SO_2 and SA
606 concentrations in the Po Valley could possibly be attributed to differences of air masses, as indicated
607 by higher RH on non-NPF days (53%) than on NPF days (38%) but similar temperature (NPF days:
608 288 K, non-NPF days: 287 K). On higher RH days, photochemistry may be suppressed, potentially
609 reducing the formation of sulfuric acid and low volatile condensable vapors.

610 The overall CS in spring (median: $8.9 \times 10^{-3} \text{ s}^{-1}$) in the Po Valley was lower than that in other polluted
611 cities ($1.5 \times 10^{-1} \text{ s}^{-1}$ – $2.0 \times 10^{-1} \text{ s}^{-1}$), but significantly higher than that in clean environments ($2.0 \times 10^{-4} \text{ s}^{-1}$
612 (Hyytiälä and Jungfrauoch) – $3.0 \times 10^{-3} \text{ s}^{-1}$ (Chacaltaya with the influence of volcanoes), Fig. 5e).
613 Contrary to Beijing or Shanghai where CS levels and efficiencies are the dominant factors for the NPF
614 process (Du et al., 2022), NPF events in Po Valley are not strongly dependent on the CS levels (9.4×10^{-3}
615 s^{-1} and $8.6 \times 10^{-3} \text{ s}^{-1}$ for non-NPF and NPF days, respectively), likely due to generally lower CS levels
616 than the Asian megacities (Fig. S8). The strength of precursor sources and their accumulation in the Po-
617 Valley region might thus be more important for NPF to occur than the overall pre-existing sink for those
618 precursors.

619 The average PM_{10} concentrations during the sampling period was around $8 \mu\text{g m}^{-3}$, significantly lower
620 than New Delhi ($268 \mu\text{g m}^{-3}$), Beijing ($33 \mu\text{g m}^{-3}$, (Li et al., 2019)) and Shanghai ($30 \mu\text{g m}^{-3}$, (Song et
621 al., 2023), Fig. S9). The major chemical compositions in PM_{10} in Po Valley were similar to those in
622 Beijing and Shanghai, with organics, ammonium nitrate, and ammonium sulfate being the most
623 abundant components. However, PM_{10} compositions in New Delhi differed from Po Valley and
624 megacities in China. In New Delhi, strong biomass burning emissions with a high abundance of primary
625 organics ($155 \mu\text{g m}^{-3}$, 58%) suppressed NPF events during the daytime from January to February but
626 led to nocturnal particle growth, which is not observed in other polluted areas (Mishra et al., 2023).

627 Even with similar levels of CS and total PM_{10} concentrations (NPF: $6.3 \mu\text{g m}^{-3}$ and non-NPF: $6.5 \mu\text{g m}^{-3}$
628) observed during noontime in Po Valley, the concentration of NO_3^- increased by 50% on non-NPF
629 days compared to NPF days, higher than the increase of PM_{10} (3.1%) as shown in Fig. S9. A lower CS
630 efficiency on NPF days due to lower fraction of nitrate was reported to suppress the scavenge of NPF
631 precursors in Beijing (Du et al., 2022), which may also have the similar influence in the Po Valley.

632 The observed growth rate for 7 – 15 nm particles in the Po Valley was about 5.1 nm h^{-1} , comparable to
633 other urban and remote sites (2.9 – 9.1 nm h^{-1} , Fig. 5f). The general similar growth rates among different
634 types of environments were also reported in previous studies (Deng et al., 2020), which needs further
635 investigation in future research.

636 For the basic gaseous precursors, the average concentration of NH_3 was ~ 10 ppb, which was in the same
637 range as that found in the Chinese megacities (10 – 30 ppb) and much higher than that at remote sites
638 (< 0.1 ppb, Table S1). The high NH_3 can be attributed to agricultural activities such as fertilization,
639 which were widely applied during springtime in the region. The strong interference of ammonia emitted
640 from fertilization to NPF was also observed in Quidja, an agricultural site in Southern Finland (Olin et
641 al., 2022). During our sampling period, measured DMA were too close to the detection limit of the
642 Vocus (Fig. S2), and lower than those observed in the Chinese megacities (10 – 40 ppt, Fig. 5d). In the

Formatted: Font: 11 pt, Not Bold

Formatted: Font: 11 pt, Not Bold

Formatted: Font: 11 pt, Not Bold

Deleted: Similarly, the overall SA concentrations were similar to those in polluted megacities in China (Fig. 5c), but much higher than those from the remote areas such as Hyytiälä ($9 \times 10^5 \text{ cm}^{-3}$) and the Jungfrauoch ($5 \times 10^5 \text{ cm}^{-3}$). Compared to other remote sites, Chacaltaya has a higher SA concentration ($2.3 \times 10^6 \text{ cm}^{-3}$) due to active volcanic degassing in the Andes (Zha et al., 2023). The SA concentrations on NPF days ($8.6 \times 10^6 \text{ cm}^{-3}$) were twice as high as those during the non-NPF days ($4 \times 10^6 \text{ cm}^{-3}$), potentially associated with the higher RH and CS loss during the non-NPF days. This is different from the findings from Beijing, where similar or even higher levels of SA during the non-NPF days were found (Yan et al., 2021).

Formatted: Font: 11 pt, Not Bold

Formatted: Font: 10.5 pt, Underline, Font color: Accent 6

Formatted: Font: 11 pt

Deleted:

Formatted: Font: 11 pt, Superscript

Formatted: Font: 11 pt

Deleted: no strong influence of CS was found between NPF and non-NPF days in the Po Valley, and only slightly higher CS was found during the noontime of non-NPF days (median: $9.4 \times 10^{-3} \text{ s}^{-1}$) than NPF days (median: $8.6 \times 10^{-3} \text{ s}^{-1}$). It is likely associated with the general lower CS than the Chinese megacities

Formatted: Font: 11 pt

Formatted: Font: 11 pt

Formatted: Font: 11 pt

Formatted: Font: 11 pt

Formatted: Font: 11 pt

Formatted: Font: 11 pt

Formatted: Font: 11 pt

Formatted: Font: 11 pt

Formatted: Font: 11 pt

Formatted: Font: (Default) Times New Roman, 11 pt

Formatted: Font: (Default) Times New Roman, 11 pt

Formatted: Font: (Default) Times New Roman, 11 pt

Deleted:

664 spring season, DMA in the Po Valley cannot fully stabilize all atmospheric SA clusters and hence NPF
665 is very sensitive to variations in the concentrations of the different stabilizers (NH₃, DMA, and as shown
666 by our analysis likely only to a lower extent organics). This could explain the scattered correlation
667 between the formation rate and SA concentrations on different days (Fig. 3).

668 Therefore, in the Po Valley region, the initial nucleation of frequent NPF is primarily attributed to high
669 sulfuric acid concentrations and basic molecules, including ammonia and various amines. This
670 mechanism is generally similar to what is observed in Chinese megacities. However, in the Po Valley
671 region, DMA, a typical base in anthropogenic emission-influenced areas, is insufficient to stabilize the
672 high levels of sulfuric acid, leading to the involvement of other basic molecules like additional other
673 type of amines and ammonia, likely originating from fertilization in the area. This involvement of
674 ammonia and other amines differs from Chinese megacities such as Shanghai, where high levels of
675 DMA were observed (~40 ppt, (Yao et al., 2018; Yao et al., 2016)). As insufficient DMA is available
676 to stabilize all clusters, we speculate that the clustering is therefore sensitive to the abundance of amines
677 and the variations in DMA or other amine concentrations would result in different formation rates. In
678 that sense, during our sampling period, NPF in Po Valley seems to be more sensitive to the strength of
679 certain emission sources of amines compared to megacity environments, where the clustering is
680 “saturated” with respect to DMA (i.e. proceeding at the maximum kinetically possible rate). The
681 abundant OOMs dominate the consecutive growth process, leading to a comparable GR to Chinese
682 megacities such as Beijing and Shanghai. Due to the relatively lower CS than these megacities, the
683 newly formed particles may however have a higher survival probability compared to the megacities and
684 provide more long-term surviving particles in the Po Valley, indicating a decisive role of NPF for Po-
685 Valley aerosol and PM_{2.5} concentrations.

686 4. Conclusions

687 In this study, we conducted a continuous two-month measurement campaign in the Italian Po Valley
688 during springtime, where frequent NPF events were observed on 66% of all days. Through direct ion
689 cluster measurement, kinetic models, and the comparison with the CLOUD chamber experiment, we
690 have determined that sulfuric acid-base nucleation is the dominant formation mechanism in the Po
691 Valley region. Abundant sulfuric acid and basic molecules, including amines and ammonia derived
692 from agriculture activities, provided ample precursors for NPF events. In contrast to megacity
693 environments, CS showed no significant difference between NPF event and non-event days, indicating
694 that in Po Valley it is more the abundance of precursors than the variations in the sink controlling the
695 occurrence of NPF. Furthermore, we observed that apart from DMA, a typical basic precursor, NH₃ and
696 other amines were also likely to be involved in NPF in the Po Valley. This was supported by the high
697 abundance of SA-NH₃ and SA-amine-NH₃ clusters measured by the APi-TOF during NPF events. DMA,
698 while more efficient than ammonia, was insufficient to stabilize all SA during our sampling period.
699 This resulted in a more scattered correlation between sulfuric acid concentrations and measured
700 formation rates compared to Chinese megacities. In that sense, we could show that the clustering during
701 NPF is clearly distinct between polluted megacity environments and polluted semi-urbanized regions
702 such as Po Valley. Similar to Beijing, we found that OOMs did not play a decisive role in the initial
703 cluster formations, likely due to the absence of ultra-low volatility organics (typical OOM dimers) in
704 the ions and neutral cluster measurements. However, low-volatility organics were abundant enough to
705 induce fast growth processes above 3 nm. The comparable GR and formation rates, along with lower
706 efficient CS compared to megacity environments, indicate a high survival probability for the newly
707 formed particles. Therefore, NPF is likely to play an important role in the fine particle concentrations
708 and pollution levels in the Po Valley region. Further reductions of key NPF species, including SO₂,
709 amines and NH₃, can contribute to suppressing NPF event frequency and lowering particle numbers.
710 This, in turn, would improve air quality in the Po Valley region.

711 Data availability

Deleted: ¶

Formatted: Font: (Default) Times New Roman, 11 pt

Formatted: Font: (Default) Times New Roman, 11 pt

Formatted: Font: (Default) Times New Roman, 11 pt

Deleted: Therefore, it can be concluded that the high sulfuric acid concentrations, basic molecules and formation rates may be the reason for the high frequency of NPF events in the Po Valley region. The abundant organics led to a comparable GR to Chinese megacities such as Beijing and Shanghai.

Formatted: Font: (Default) Times New Roman, 11 pt

Deleted: of the chemical composition and physical properties of newly formed particles and clusters in the Italian Po Valley during springtime. The Po Valley experienced frequent NPF events during the sampling period, occurring on approximately 66% of the days. We observed high concentrations of sulfuric acid during the NPF events, comparable to those found in Chinese megacities. The correlation between the formation rate of particles and sulfuric acid concentrations, together with the information from dimethylamine simulations and CLOUD chamber experiments, suggest that gaseous DMA might have been insufficient to stabilize all atmospheric sulfuric acid during our sampling period. Except for DMA, other amines and NH₃ were also involved in NPF in the Po Valley, which was supported by the high abundance of SA-NH₃ and SA-amine-NH₃ clusters measured by the APi-TOF on NPF days. Generally, the NPF mechanism is therefore very sensitive to the abundance of amines (e.g., DMA) with high levels of NH₃, resulting in a more scattered correlation between H₂SO₄ concentrations and measured formation rate. At the same time, OOMs do not seem to be decisive for the sub-3 nm formation process due to the lack of ultra-low volatility organics (highly oxygenated CHO compounds and dimers), however low volatility organics were abundant enough to induce fast growth processes above 3 nm. The comparable GR and formation rate, but lower CS compared to other polluted environments,

Formatted: Font: (Default) Times New Roman, 11 pt

746 Data are available from the authors upon request.

747 **Competing interests**

748 At least one of the (co-)authors is a member of the editorial board of Atmospheric Chemistry and
749 Physics

750 **Author contributions**

751 JC, DS, FB, and MK designed the research. JC, JS, YFG, SH, MP, AN, FM, SD, MR, NZ and CM
752 collected the data at the SPC site. JC, JS, YG, ST, RY, DA, QZ, DS and FB interpreted the data. MP,
753 WH, YL, GC, LQ, KL, YG, CW, WN, JK, CM, QZ, DS, FB helped to improve the manuscript. JC, JS,
754 DS, and FB wrote the manuscript with contributions from all co-authors. All authors have given
755 approval to the final version of this manuscript.

756 **Acknowledgements**

757 The work is supported by the Academy of Finland (Center of Excellence in Atmospheric Sciences,
758 project no. 307331, PROF13 funding no. 311932, and ACCC Flagship no. 337549), the European
759 Research Council via ATM-GTP (no. 742206), Consolidator grant INTEGRATE (no. 865799) and
760 CHAPAs (no. 850614), the European Union's Horizon 2020 research and innovation programme
761 (project FORCeS under grant agreement no. 821205, H2020-INFRAIA-2020-1 grant agreement no.
762 101008004, Marie Skłodowska–Curie grant agreement no. 895875 (NPF-PANDA), the Vienna Science
763 and Technology Fund (WWTF) through project VRG22-003, Jenny and Antti Wihuri Foundation, and
764 the Knut and Alice Wallenberg Foundation (WAF project CLOUDFORM, grant no. 2017.0165). The
765 authors also would like to thank the effort from all the researchers in the SPC site. The authors would
766 also like to thank Chenjuan Deng, Mao Xiao and Lubna Dada for providing the supporting data in
767 Beijing and CLOUD chamber experiment.

768

769 **Reference**

- 770 Almeida, J., Schobesberger, S., Kurten, A., Ortega, I. K., Kupiainen-Maatta, O., Praplan, A. P., Adamov,
771 A., Amorim, A., Bianchi, F., Breitenlechner, M., David, A., Dommen, J., Donahue, N. M., Downard, A.,
772 Dunne, E., Duplissy, J., Ehrhart, S., Flagan, R. C., Franchin, A., Guida, R., Hakala, J., Hansel, A.,
773 Heinritzi, M., Henschel, H., Jokinen, T., Junninen, H., Kajos, M., Kangasluoma, J., Keskinen, H., Kupc,
774 A., Kurten, T., Kvashin, A. N., Laaksonen, A., Lehtipalo, K., Leiminger, M., Leppa, J., Loukonen, V.,
775 Makhmutov, V., Mathot, S., McGrath, M. J., Nieminen, T., Olenius, T., Onnela, A., Petaja, T.,
776 Riccobono, F., Riipinen, I., Rissanen, M., Rondo, L., Ruuskanen, T., Santos, F. D., Sarnela, N.,
777 Schallhart, S., Schnitzhofer, R., Seinfeld, J. H., Simon, M., Sipila, M., Stozhkov, Y., Stratmann, F.,
778 Tome, A., Trostl, J., Tsagkogeorgas, G., Vaattovaara, P., Viisanen, Y., Virtanen, A., Vrtala, A., Wagner,
779 P. E., Weingartner, E., Wex, H., Williamson, C., Wimmer, D., Ye, P., Yli-Juuti, T., Carslaw, K. S.,
780 Kulmala, M., Curtius, J., Baltensperger, U., Worsnop, D. R., Vehkamäki, H., and Kirkby, J.: Molecular
781 understanding of sulphuric acid-amine particle nucleation in the atmosphere, *Nature*, 502, 359-363,
782 10.1038/nature12663, 2013.
- 783 Boulon, J., Sellegri, K., Venzac, H., Picard, D., Weingartner, E., Wehrle, G., Collaud Coen, M.,
784 Bütikofer, R., Flückiger, E., Baltensperger, U., and Laj, P.: New particle formation and ultrafine
785 charged aerosol climatology at a high altitude site in the Alps (Jungfraujoch, 3580 m a.s.l.,
786 Switzerland), *Atmospheric Chemistry and Physics*, 10, 9333-9349, 10.5194/acp-10-9333-2010, 2010.
- 787 Brean, J., Beddows, D. C. S., Shi, Z., Temime-Roussel, B., Marchand, N., Querol, X., Alastuey, A.,
788 Minguillón, M. C., and Harrison, R. M.: Molecular insights into new particle formation in Barcelona,
789 Spain, *Atmospheric Chemistry and Physics*, 20, 10029-10045, 10.5194/acp-20-10029-2020, 2020.
- 790 Cai, J., Daellenbach, K. R., Wu, C., Zheng, Y., Zheng, F., Du, W., Haslett, S. L., Chen, Q., Kulmala, M.,
791 and Mohr, C.: Characterization of offline analysis of particulate matter with FIGAERO-CIMS,
792 *Atmospheric Measurement Techniques*, 16, 1147-1165, 10.5194/amt-16-1147-2023, 2023a.
- 793 Cai, J., Wu, C., Wang, J., Du, W., Zheng, F., Hakala, S., Fan, X., Chu, B., Yao, L., Feng, Z., Liu, Y., Sun, Y.,
794 Zheng, J., Yan, C., Bianchi, F., Kulmala, M., Mohr, C., and Daellenbach, K. R.: Influence of organic
795 aerosol molecular composition on particle absorptive properties in autumn Beijing, *Atmospheric
796 Chemistry and Physics*, 22, 1251-1269, 10.5194/acp-22-1251-2022, 2022.
- 797 Cai, R., Attoui, M., Jiang, J., Korhonen, F., Hao, J., Petäjä, T., and Kangasluoma, J.: Characterization of
798 a high-resolution supercritical differential mobility analyzer at reduced flow rates, *Aerosol Science
799 and Technology*, 52, 1332-1343, 10.1080/02786826.2018.1520964, 2018.
- 800 Cai, R., Yang, D., Fu, Y., Wang, X., Li, X., Ma, Y., Hao, J., Zheng, J., and Jiang, J.: Aerosol surface area
801 concentration: a governing factor in new particle formation in Beijing, *Atmospheric Chemistry and
802 Physics*, 17, 12327-12340, 10.5194/acp-17-12327-2017, 2017.
- 803 Cai, R., Yin, R., Li, X., Xie, H.-B., Yang, D., Kerminen, V.-M., Smith, J. N., Ma, Y., Hao, J., Chen, J.,
804 Kulmala, M., Zheng, J., Jiang, J., and Elm, J.: Significant contributions of trimethylamine to sulfuric
805 acid nucleation in polluted environments, *npj Climate and Atmospheric Science*, 6, 10.1038/s41612-
806 023-00405-3, 2023b.
- 807 Cai, R., Yan, C., Yang, D., Yin, R., Lu, Y., Deng, C., Fu, Y., Ruan, J., Li, X., Kontkanen, J., Zhang, Q.,
808 Kangasluoma, J., Ma, Y., Hao, J., Worsnop, D. R., Bianchi, F., Paasonen, P., Kerminen, V. M., Liu, Y.,
809 Wang, L., Zheng, J., Kulmala, M., and Jiang, J.: Sulfuric acid-amine nucleation in urban Beijing,
810 *Atmos. Chem. Phys.*, 21, 2457-2468, 10.5194/acp-21-2457-2021, 2021.
- 811 Chu, B., Kerminen, V.-M., Bianchi, F., Yan, C., Petäjä, T., and Kulmala, M.: Atmospheric new particle
812 formation in China, *Atmospheric Chemistry and Physics*, 19, 115-138, 10.5194/acp-19-115-2019,
813 2019.
- 814 Dada, L., Chellapermal, R., Buenrostro Mazon, S., Paasonen, P., Lampilahti, J., Manninen, H. E.,
815 Junninen, H., Petäjä, T., Kerminen, V.-M., and Kulmala, M.: Refined classification and
816 characterization of atmospheric new-particle formation events using air ions, *Atmospheric
817 Chemistry and Physics*, 18, 17883-17893, 10.5194/acp-18-17883-2018, 2018.
- 818 Dai, L., Wang, H., Zhou, L., An, J., Tang, L., Lu, C., Yan, W., Liu, R., Kong, S., Chen, M., Lee, S., and Yu,
819 H.: Regional and local new particle formation events observed in the Yangtze River Delta region,

820 China, *Journal of Geophysical Research: Atmospheres*, 122, 2389-2402, 10.1002/2016jd026030,
821 2017.

822 Dal Maso, M., Kulmala, M., Riipinen, I., Wagner, R., Hussein, T., Aalto, P. P., and Lehtinen, K. E. J.:
823 Formation and growth of fresh atmospheric aerosols: eight years of aerosol size distribution data
824 from SMEAR II, Hyytiälä, Finland, *Boreal Environment Research*, 10, 323-336, 2005.

825 de Jesus, A. L., Rahman, M. M., Mazaheri, M., Thompson, H., Knibbs, L. D., Jeong, C., Evans, G., Nei,
826 W., Ding, A., Qiao, L., Li, L., Portin, H., Niemi, J. V., Timonen, H., Luoma, K., Petaja, T., Kulmala, M.,
827 Kowalski, M., Peters, A., Cyrus, J., Ferrero, L., Manigrasso, M., Avino, P., Buonano, G., Reche, C.,
828 Querol, X., Beddows, D., Harrison, R. M., Sowlat, M. H., Sioutas, C., and Morawska, L.: Ultrafine
829 particles and PM(2.5) in the air of cities around the world: Are they representative of each other?,
830 *Environ Int*, 129, 118-135, 10.1016/j.envint.2019.05.021, 2019.

831 Decesari, S., Allan, J., Plass-Duelmer, C., Williams, B. J., Paglione, M., Facchini, M. C., O'Dowd, C.,
832 Harrison, R. M., Giet, J. K., Coe, H., Giulianelli, L., Gobbi, G. P., Lanconelli, C., Carbone, C., Worsnop,
833 D., Lambe, A. T., Ahern, A. T., Moretti, F., Tagliavini, E., Elste, T., Gilge, S., Zhang, Y., and Dall'Osto,
834 M.: Measurements of the aerosol chemical composition and mixing state in the Po Valley using
835 multiple spectroscopic techniques, *Atmospheric Chemistry and Physics*, 14, 12109-12132,
836 10.5194/acp-14-12109-2014, 2014.

837 Deng, C., Fu, Y., Dada, L., Yan, C., Cai, R., Yang, D., Zhou, Y., Yin, R., Lu, Y., Li, X., Qiao, X., Fan, X., Nie,
838 W., Kontkanen, J., Kangasluoma, J., Chu, B., Ding, A., Kerminen, V. M., Paasonen, P., Worsnop, D. R.,
839 Bianchi, F., Liu, Y., Zheng, J., Wang, L., Kulmala, M., and Jiang, J.: Seasonal Characteristics of New
840 Particle Formation and Growth in Urban Beijing, *Environ Sci Technol*, 54, 8547-8557,
841 10.1021/acs.est.0c00808, 2020.

842 Du, W., Cai, J., Zheng, F., Yan, C., Zhou, Y., Guo, Y., Chu, B., Yao, L., Heikkinen, L. M., Fan, X., Wang, Y.,
843 Cai, R., Hakala, S., Chan, T., Kontkanen, J., Tuovinen, S., Petäjä, T., Kangasluoma, J., Bianchi, F.,
844 Paasonen, P., Sun, Y., Kerminen, V.-M., Liu, Y., Daellenbach, K. R., Dada, L., and Kulmala, M.:
845 Influence of Aerosol Chemical Composition on Condensation Sink Efficiency and New Particle
846 Formation in Beijing, *Environmental Science & Technology Letters*, 9, 375-382,
847 10.1021/acs.estlett.2c00159, 2022.

848 Fan, X., Cai, J., Yan, C., Zhao, J., Guo, Y., Li, C., Dällenbach, K. R., Zheng, F., Lin, Z., Chu, B., Wang, Y.,
849 Dada, L., Zha, Q., Du, W., Kontkanen, J., Kurtén, T., Iyer, S., Kujansuu, J. T., Petäjä, T., Worsnop, D. R.,
850 Kerminen, V.-M., Liu, Y., Bianchi, F., Tham, Y. J., Yao, L., and Kulmala, M.: Atmospheric gaseous
851 hydrochloric and hydrobromic acid in urban Beijing, China: detection, source identification and
852 potential atmospheric impacts, *Atmospheric Chemistry and Physics*, 21, 11437-11452, 10.5194/acp-
853 21-11437-2021, 2021.

854 Fernández de la Mora, J. and Kozlowski, J.: Hand-held differential mobility analyzers of high
855 resolution for 1–30nm particles: Design and fabrication considerations, *Journal of Aerosol Science*,
856 57, 45-53, 10.1016/j.jaerosci.2012.10.009, 2013.

857 Fu, Y., Xue, M., Cai, R., Kangasluoma, J., and Jiang, J.: Theoretical and experimental analysis of the
858 core sampling method: Reducing diffusional losses in aerosol sampling line, *Aerosol Science and*
859 *Technology*, 53, 793-801, 10.1080/02786826.2019.1608354, 2019.

860 Gilardoni, S., Massoli, P., Paglione, M., Giulianelli, L., Carbone, C., Rinaldi, M., Decesari, S., Sandrini,
861 S., Costabile, F., Gobbi, G. P., Pietrogrande, M. C., Visentin, M., Scotto, F., Fuzzi, S., and Facchini, M.
862 C.: Direct observation of aqueous secondary organic aerosol from biomass-burning emissions, *Proc*
863 *Natl Acad Sci U S A*, 113, 10013-10018, 10.1073/pnas.1602212113, 2016.

864 Guo, S., Hu, M., Zamora, M. L., Peng, J., Shang, D., Zheng, J., Du, Z., Wu, Z., Shao, M., Zeng, L.,
865 Molina, M. J., and Zhang, R.: Elucidating severe urban haze formation in China, *Proc Natl Acad Sci U S*
866 *A*, 111, 17373-17378, 10.1073/pnas.1419604111, 2014.

867 Guo, S., Hu, M., Peng, J., Wu, Z., Zamora, M. L., Shang, D., Du, Z., Zheng, J., Fang, X., Tang, R., Wu, Y.,
868 Zeng, L., Shuai, S., Zhang, W., Wang, Y., Ji, Y., Li, Y., Zhang, A. L., Wang, W., Zhang, F., Zhao, J., Gong,
869 X., Wang, C., Molina, M. J., and Zhang, R.: Remarkable nucleation and growth of ultrafine particles

870 from vehicular exhaust, *Proceedings of the National Academy of Sciences*,
871 10.1073/pnas.1916366117, 2020.
872 Guo, Y., Yan, C., Liu, Y., Qiao, X., Zheng, F., Zhang, Y., Zhou, Y., Li, C., Fan, X., Lin, Z., Feng, Z., Zhang,
873 Y., Zheng, P., Tian, L., Nie, W., Wang, Z., Huang, D., Daellenbach, K. R., Yao, L., Dada, L., Bianchi, F.,
874 Jiang, J., Liu, Y., Kerminen, V.-M., and Kulmala, M.: Seasonal variation in oxygenated organic
875 molecules in urban Beijing and their contribution to secondary organic aerosol, *Atmospheric*
876 *Chemistry and Physics*, 22, 10077-10097, 10.5194/acp-22-10077-2022, 2022.
877 Hamed, A., Joutsensaari, J., Mikkonen, S., Sogacheva, L., Dal Maso, M., Kulmala, M., Cavalli, F., Fuzzi,
878 S., Facchini, M. C., Decesari, S., Mircea, M., Lehtinen, K. E. J., and Laaksonen, A.: Nucleation and
879 growth of new particles in Po Valley, Italy, *Atmos. Chem. Phys.*, 7, 355-376, 10.5194/acp-7-355-2007,
880 2007.
881 Harrison, M. A. J., Barra, S., Borghesi, D., Vione, D., Arsene, C., and Iulian Olariu, R.: Nitrated phenols
882 in the atmosphere: a review, *Atmospheric Environment*, 39, 231-248,
883 10.1016/j.atmosenv.2004.09.044, 2005.
884 He, X. C., Tham, Y. J., Dada, L., Wang, M., Finkenzeller, H., Stolzenburg, D., Iyer, S., Simon, M., Kurten,
885 A., Shen, J., Rorup, B., Rissanen, M., Schobesberger, S., Baalbaki, R., Wang, D. S., Koenig, T. K.,
886 Jokinen, T., Sarnela, N., Beck, L. J., Almeida, J., Amanatidis, S., Amorim, A., Ataei, F., Baccharini, A.,
887 Bertozzi, B., Bianchi, F., Brilke, S., Caudillo, L., Chen, D., Chiu, R., Chu, B., Dias, A., Ding, A., Dommen,
888 J., Duplissy, J., El Haddad, I., Gonzalez Carracedo, L., Granzin, M., Hansel, A., Heinritzi, M., Hofbauer,
889 V., Junninen, H., Kangasluoma, J., Kemppainen, D., Kim, C., Kong, W., Krechmer, J. E., Kvashin, A.,
890 Laitinen, T., Lamkaddam, H., Lee, C. P., Lehtipalo, K., Leiminger, M., Li, Z., Makhmutov, V., Manninen,
891 H. E., Marie, G., Marten, R., Mathot, S., Mauldin, R. L., Mentler, B., Mohler, O., Muller, T., Nie, W.,
892 Onnela, A., Petaja, T., Pfeifer, J., Philipppov, M., Ranjithkumar, A., Saiz-Lopez, A., Salma, I., Scholz, W.,
893 Schuchmann, S., Schulze, B., Steiner, G., Stozhkov, Y., Tauber, C., Tome, A., Thakur, R. C., Vaisanen,
894 O., Vazquez-Pufleau, M., Wagner, A. C., Wang, Y., Weber, S. K., Winkler, P. M., Wu, Y., Xiao, M., Yan,
895 C., Ye, Q., Ylisirnio, A., Zauner-Wieczorek, M., Zha, Q., Zhou, P., Flagan, R. C., Curtius, J.,
896 Baltensperger, U., Kulmala, M., Kerminen, V. M., Kurten, T., Donahue, N. M., Volkamer, R., Kirkby, J.,
897 Worsnop, D. R., and Sipila, M.: Role of iodine oxoacids in atmospheric aerosol nucleation, *Science*,
898 371, 589-595, 10.1126/science.abe0298, 2021.
899 Jokinen, T., Sipilä, M., Junninen, H., Ehn, M., Lönn, G., Hakala, J., Petäjä, T., Mauldin, R. L., Kulmala,
900 M., and Worsnop, D. R.: Atmospheric sulphuric acid and neutral cluster measurements using CI-API-
901 TOF, *Atmospheric Chemistry and Physics*, 12, 4117-4125, 10.5194/acp-12-4117-2012, 2012.
902 Junninen, H., Ehn, M., Petäjä, T., Luosujärvi, L., Kotiaho, T., Kostianen, R., Rohner, U., Gonin, M.,
903 Fuhrer, K., Kulmala, M., and Worsnop, D. R.: A high-resolution mass spectrometer to measure
904 atmospheric ion composition, *Atmospheric Measurement Techniques*, 3, 1039-1053, 10.5194/amt-
905 3-1039-2010, 2010.
906 Kangasluoma, J., Ahonen, L. R., Laurila, T. M., Cai, R., Enroth, J., Mazon, S. B., Korhonen, F., Aalto, P.
907 P., Kulmala, M., Attoui, M., and Petäjä, T.: Laboratory verification of a new high flow differential
908 mobility particle sizer, and field measurements in Hyytiälä, *Journal of Aerosol Science*, 124, 1-9,
909 10.1016/j.jaerosci.2018.06.009, 2018.
910 Kangasluoma, J., Attoui, M., Junninen, H., Lehtipalo, K., Samodurov, A., Korhonen, F., Sarnela, N.,
911 Schmidt-Ott, A., Worsnop, D., Kulmala, M., and Petäjä, T.: Sizing of neutral sub 3nm tungsten oxide
912 clusters using Airmodus Particle Size Magnifier, *Journal of Aerosol Science*, 87, 53-62,
913 10.1016/j.jaerosci.2015.05.007, 2015.
914 Kangasluoma, J., Franchin, A., Duplissy, J., Ahonen, L., Korhonen, F., Attoui, M., Mikkilä, J., Lehtipalo,
915 K., Vanhanen, J., Kulmala, M., and Petäjä, T.: Operation of the Airmodus A11 nano Condensation
916 Nucleus Counter at various
917 inlet pressures and various operation temperatures, and design of a new inlet
918 system, *Atmospheric Measurement Techniques*, 9, 2977-2988, 10.5194/amt-9-2977-2016, 2016.

919 Kirkby, J., Curtius, J., Almeida, J., Dunne, E., Duplissy, J., Ehrhart, S., Franchin, A., Gagne, S., Ickes, L.,
920 Kurten, A., Kupc, A., Metzger, A., Riccobono, F., Rondo, L., Schobesberger, S., Tsagkogeorgas, G.,
921 Wimmer, D., Amorim, A., Bianchi, F., Breitenlechner, M., David, A., Dommen, J., Downard, A., Ehn,
922 M., Flagan, R. C., Haider, S., Hansel, A., Hauser, D., Jud, W., Junninen, H., Kreissl, F., Kvashin, A.,
923 Laaksonen, A., Lehtipalo, K., Lima, J., Lovejoy, E. R., Makhmutov, V., Mathot, S., Mikkilä, J.,
924 Minginette, P., Mogo, S., Nieminen, T., Onnela, A., Pereira, P., Petaja, T., Schnitzhofer, R., Seinfeld, J.
925 H., Sipila, M., Stozhkov, Y., Stratmann, F., Tome, A., Vanhanen, J., Viisanen, Y., Vrtala, A., Wagner, P.
926 E., Walther, H., Weingartner, E., Wex, H., Winkler, P. M., Carslaw, K. S., Worsnop, D. R.,
927 Baltensperger, U., and Kulmala, M.: Role of sulphuric acid, ammonia and galactic cosmic rays in
928 atmospheric aerosol nucleation, *Nature*, 476, 429-433, 10.1038/nature10343, 2011.

929 Kirkby, J., Duplissy, J., Sengupta, K., Frege, C., Gordon, H., Williamson, C., Heinritzi, M., Simon, M.,
930 Yan, C., Almeida, J., Trostl, J., Nieminen, T., Ortega, I. K., Wagner, R., Adamov, A., Amorim, A.,
931 Bernhammer, A. K., Bianchi, F., Breitenlechner, M., Brilke, S., Chen, X., Craven, J., Dias, A., Ehrhart, S.,
932 Flagan, R. C., Franchin, A., Fuchs, C., Guida, R., Hakala, J., Hoyle, C. R., Jokinen, T., Junninen, H.,
933 Kangasluoma, J., Kim, J., Krapf, M., Kurten, A., Laaksonen, A., Lehtipalo, K., Makhmutov, V., Mathot,
934 S., Molteni, U., Onnela, A., Perakyla, O., Piel, F., Petaja, T., Praplan, A. P., Pringle, K., Rap, A.,
935 Richards, N. A., Riipinen, I., Rissanen, M. P., Rondo, L., Sarnela, N., Schobesberger, S., Scott, C. E.,
936 Seinfeld, J. H., Sipila, M., Steiner, G., Stozhkov, Y., Stratmann, F., Tome, A., Virtanen, A., Vogel, A. L.,
937 Wagner, A. C., Wagner, P. E., Weingartner, E., Wimmer, D., Winkler, P. M., Ye, P., Zhang, X., Hansel,
938 A., Dommen, J., Donahue, N. M., Worsnop, D. R., Baltensperger, U., Kulmala, M., Carslaw, K. S., and
939 Curtius, J.: Ion-induced nucleation of pure biogenic particles, *Nature*, 533, 521-526,
940 10.1038/nature17953, 2016.

941 Kontkanen, J., Järvinen, E., Manninen, H. E., Lehtipalo, K., Kangasluoma, J., Decesari, S., Gobbi, G. P.,
942 Laaksonen, A., Petäjä, T., and Kulmala, M.: High concentrations of sub-3nm clusters and frequent
943 new particle formation observed in the Po Valley, Italy, during the PEGASOS 2012 campaign,
944 *Atmospheric Chemistry and Physics*, 16, 1919-1935, 10.5194/acp-16-1919-2016, 2016.

945 Kontkanen, J., Lehtipalo, K., Ahonen, L., Kangasluoma, J., Manninen, H. E., Hakala, J., Rose, C.,
946 Sellegri, K., Xiao, S., Wang, L., Qi, X., Nie, W., Ding, A., Yu, H., Lee, S., Kerminen, V.-M., Petäjä, T., and
947 Kulmala, M.: Measurements of sub-3 nm particles using a particle size magnifier in different
948 environments: from clean mountain top to polluted megacities, *Atmospheric Chemistry and Physics*,
949 17, 2163-2187, 10.5194/acp-17-2163-2017, 2017.

950 Kulmala, M., Kerminen, V. M., Petäjä, T., Ding, A. J., and Wang, L.: Atmospheric gas-to-particle
951 conversion: why NPF events are observed in megacities?, *Faraday Discussions*, 200, 271-288,
952 10.1039/C6FD00257A, 2017.

953 Kulmala, M., Petäjä, T., Nieminen, T., Sipilä, M., Manninen, H. E., Lehtipalo, K., Dal Maso, M., Aalto,
954 P. P., Junninen, H., Paasonen, P., Riipinen, I., Lehtinen, K. E. J., Laaksonen, A., and Kerminen, V.-M.:
955 Measurement of the nucleation of atmospheric aerosol particles, *Nature Protocols*, 7, 1651-1667,
956 10.1038/nprot.2012.091, 2012.

957 Kulmala, M., Junninen, H., Dada, L., Salma, I., Weidinger, T., Thén, W., Vörösmarty, M., Komsaare, K.,
958 Stolzenburg, D., Cai, R., Yan, C., Li, X., Deng, C., Jiang, J., Petäjä, T., Nieminen, T., and Kerminen, V.-
959 M.: Quiet New Particle Formation in the Atmosphere, *Frontiers in Environmental Science*, 10,
960 10.3389/fenvs.2022.912385, 2022.

961 Kulmala, M., Kontkanen, J., Junninen, H., Lehtipalo, K., Manninen, H. E., Nieminen, T., Petäjä, T.,
962 Sipilä, M., Schobesberger, S., Rantala, P., Franchin, A., Jokinen, T., Järvinen, E., Äijälä, M.,
963 Kangasluoma, J., Hakala, J., Aalto, P. P., Paasonen, P., Mikkilä, J., Vanhanen, J., Aalto, J., Hakola, H.,
964 Makkonen, U., Ruuskanen, T., Mauldin, R. L., Duplissy, J., Vehkamäki, H., Bäck, J., Kortelainen, A.,
965 Riipinen, I., Kurtén, T., Johnston, M. V., Smith, J. N., Ehn, M., Mentel, T. F., Lehtinen, K. E. J.,
966 Laaksonen, A., Kerminen, V.-M., and Worsnop, D. R.: Direct Observations of Atmospheric Aerosol
967 Nucleation, *Science*, 339, 943-946, 10.1126/science.1227385, 2013.

968 Kulmala, M., Dada, L., Daellenbach, K. R., Yan, C., Stolzenburg, D., Kontkanen, J., Ezhova, E., Hakala,
969 S., Tuovinen, S., Kokkonen, T. V., Kurppa, M., Cai, R., Zhou, Y., Yin, R., Baalbaki, R., Chan, T., Chu, B.,

970 Deng, C., Fu, Y., Ge, M., He, H., Heikkinen, L., Junninen, H., Liu, Y., Lu, Y., Nie, W., Rusanen, A.,
971 Vakkari, V., Wang, Y., Yang, G., Yao, L., Zheng, J., Kujansuu, J., Kangasluoma, J., Petaja, T., Paasonen,
972 P., Jarvi, L., Worsnop, D., Ding, A., Liu, Y., Wang, L., Jiang, J., Bianchi, F., and Kerminen, V. M.: Is
973 reducing new particle formation a plausible solution to mitigate particulate air pollution in Beijing
974 and other Chinese megacities?, *Faraday Discuss*, 226, 334-347, 10.1039/d0fd00078g, 2021.
975 Kurten, A., Rondo, L., Ehrhart, S., and Curtius, J.: Calibration of a chemical ionization mass
976 spectrometer for the measurement of gaseous sulfuric acid, *J Phys Chem A*, 116, 6375-6386,
977 10.1021/jp212123n, 2012.
978 Lampimäki, M., Baalbaki, R., Ahonen, L., Korhonen, F., Cai, R., Chan, T., Stolzenburg, D., Petäjä, T.,
979 Kangasluoma, J., Vanhanen, J., and Lehtipalo, K.: Novel aerosol diluter – Size dependent
980 characterization down to 1 nm particle size, *Journal of Aerosol Science*, 172, 106180,
981 <https://doi.org/10.1016/j.jaerosci.2023.106180>, 2023.
982 Lehtipalo, K., Ahonen, L. R., Baalbaki, R., Sulo, J., Chan, T., Laurila, T., Dada, L., Duplissy, J., Miettinen,
983 E., Vanhanen, J., Kangasluoma, J., Kulmala, M., Petäjä, T., and Jokinen, T.: The standard operating
984 procedure for Airmodus Particle Size Magnifier and nano-Condensation Nucleus Counter, *Journal of*
985 *Aerosol Science*, 159, 10.1016/j.jaerosci.2021.105896, 2022.
986 Lehtipalo, K., Yan, C., Dada, L., Bianchi, F., Xiao, M., Wagner, R., Stolzenburg, D., Ahonen, L. R.,
987 Amorim, A., Baccarini, A., Bauer, P. S., Baumgartner, B., Bergen, A., Bernhammer, A.-K.,
988 Breitenlechner, M., Brilke, S., Buchholz, A., Mazon, S. B., Chen, D., Chen, X., Dias, A., Dommen, J.,
989 Draper, D. C., Duplissy, J., Ehn, M., Finkenzeller, H., Fischer, L., Frege, C., Fuchs, C., Garmash, O.,
990 Gordon, H., Hakala, J., He, X., Heikkinen, L., Heinritzi, M., Helm, J. C., Hofbauer, V., Hoyle, C. R.,
991 Jokinen, T., Kangasluoma, J., Kerminen, V.-M., Kim, C., Kirkby, J., Kontkanen, J., Kürten, A., Lawler, M.
992 J., Mai, H., Mathot, S., Mauldin, R. L., Molteni, U., Nichman, L., Nie, W., Nieminen, T., Ojdanic, A.,
993 Onnela, A., Passananti, M., Petäjä, T., Piel, F., Pospisilova, V., Quéléver, L. L. J., Rissanen, M. P., Rose,
994 C., Sarnela, N., Schallhart, S., Schuchmann, S., Sengupta, K., Simon, M., Sipilä, M., Tauber, C., Tomé,
995 A., Tröstl, J., Väisänen, O., Vogel, A. L., Volkamer, R., Wagner, A. C., Wang, M., Weitz, L., Wimmer, D.,
996 Ye, P., Ylisirniö, A., Zha, Q., Carslaw, K. S., Curtius, J., Donahue, N. M., Flagan, R. C., Hansel, A.,
997 Ripinen, I., Virtanen, A., Winkler, P. M., Baltensperger, U., Kulmala, M., and Worsnop, D. R.:
998 Multicomponent new particle formation from sulfuric acid, ammonia, and biogenic vapors, *Science*
999 *Advances*, 4, eaau5363, doi:10.1126/sciadv.aau5363, 2018.
1000 Li, H., Cheng, J., Zhang, Q., Zheng, B., Zhang, Y., Zheng, G., and He, K.: Rapid transition in winter
1001 aerosol composition in Beijing from 2014 to 2017: response to clean air actions, *Atmospheric*
1002 *Chemistry and Physics*, 19, 11485-11499, 10.5194/acp-19-11485-2019, 2019.
1003 Liu, S., Hu, M., Wu, Z., Wehner, B., Wiedensohler, A., and Cheng, Y.: Aerosol number size distribution
1004 and new particle formation at a rural/coastal site in Pearl River Delta (PRD) of China, *Atmospheric*
1005 *Environment*, 42, 6275-6283, 10.1016/j.atmosenv.2008.01.063, 2008.
1006 Manninen, H. E., Nieminen, T., Asmi, E., Gagné, S., Häkkinen, S., Lehtipalo, K., Aalto, P., Vana, M.,
1007 Mirme, A., Mirme, S., Hörrak, U., Plass-Dülmer, C., Stange, G., Kiss, G., Hoffer, A., Törö, N., Moerman,
1008 M., Henzing, B., de Leeuw, G., Brinkenberg, M., Kouvarakis, G. N., Bougiatioti, A., Mihalopoulos, N.,
1009 O'Dowd, C., Ceburnis, D., Arneth, A., Svenningsson, B., Swietlicki, E., Tarozzi, L., Decesari, S., Facchini,
1010 M. C., Birmili, W., Sonntag, A., Wiedensohler, A., Boulon, J., Sellegri, K., Laj, P., Gysel, M., Bukowiecki,
1011 N., Weingartner, E., Wehrle, G., Laaksonen, A., Hamed, A., Joutsensaari, J., Petäjä, T., Kerminen, V.
1012 M., and Kulmala, M.: EUCAARI ion spectrometer measurements at 12 European sites – analysis of
1013 new particle formation events, *Atmos. Chem. Phys.*, 10, 7907-7927, 10.5194/acp-10-7907-2010,
1014 2010.
1015 Mishra, S., Tripathi, S. N., Kanawade, V. P., Haslett, S. L., Dada, L., Ciarelli, G., Kumar, V., Singh, A.,
1016 Bhattu, D., Rastogi, N., Daellenbach, K. R., Ganguly, D., Gargava, P., Slowik, J. G., Kulmala, M., Mohr,
1017 C., El-Haddad, I., and Prevot, A. S. H.: Rapid night-time nanoparticle growth in Delhi driven by
1018 biomass-burning emissions, *Nature Geoscience*, 16, 224-230, 10.1038/s41561-023-01138-x, 2023.
1019 Mohr, C., Lopez-Hilfiker, F. D., Zotter, P., Prevot, A. S., Xu, L., Ng, N. L., Herndon, S. C., Williams, L. R.,
1020 Franklin, J. P., Zahniser, M. S., Worsnop, D. R., Knighton, W. B., Aiken, A. C., Gorkowski, K. J., Dubey,

1021 M. K., Allan, J. D., and Thornton, J. A.: Contribution of nitrated phenols to wood burning brown
1022 carbon light absorption in Detling, United Kingdom during winter time, *Environ Sci Technol*, 47,
1023 6316-6324, 10.1021/es400683v, 2013.

1024 Nie, W., Yan, C., Huang, D. D., Wang, Z., Liu, Y., Qiao, X., Guo, Y., Tian, L., Zheng, P., Xu, Z., Li, Y., Xu,
1025 Z., Qi, X., Sun, P., Wang, J., Zheng, F., Li, X., Yin, R., Dallenbach, K. R., Bianchi, F., Petäjä, T., Zhang, Y.,
1026 Wang, M., Schervish, M., Wang, S., Qiao, L., Wang, Q., Zhou, M., Wang, H., Yu, C., Yao, D., Guo, H.,
1027 Ye, P., Lee, S., Li, Y. J., Liu, Y., Chi, X., Kerminen, V.-M., Ehn, M., Donahue, N. M., Wang, T., Huang, C.,
1028 Kulmala, M., Worsnop, D., Jiang, J., and Ding, A.: Secondary organic aerosol formed by condensing
1029 anthropogenic vapours over China's megacities, *Nature Geoscience*, 15, 255-261, 10.1038/s41561-
1030 022-00922-5, 2022.

1031 Paasonen, P., Nieminen, T., Asmi, E., Manninen, H. E., Petäjä, T., Plass-Dülmer, C., Flentje, H., Birmili,
1032 W., Wiedensohler, A., Hörrak, U., Metzger, A., Hamed, A., Laaksonen, A., Facchini, M. C., Kerminen,
1033 V. M., and Kulmala, M.: On the roles of sulphuric acid and low-volatility organic vapours in the initial
1034 steps of atmospheric new particle formation, *Atmospheric Chemistry and Physics*, 10, 11223-11242,
1035 10.5194/acp-10-11223-2010, 2010.

1036 Paglione, M., Decesari, S., Rinaldi, M., Tarozzi, L., Manarini, F., Gilardoni, S., Facchini, M. C., Fuzzi, S.,
1037 Bacco, D., Trentini, A., Pandis, S. N., and Nenes, A.: Historical Changes in Seasonal Aerosol Acidity in
1038 the Po Valley (Italy) as Inferred from Fog Water and Aerosol Measurements, *Environ Sci Technol*, 55,
1039 7307-7315, 10.1021/acs.est.1c00651, 2021.

1040 Paglione, M., Saarikoski, S., Carbone, S., Hillamo, R., Facchini, M. C., Finessi, E., Giulianelli, L.,
1041 Carbone, C., Fuzzi, S., Moretti, F., Tagliavini, E., Swietlicki, E., Eriksson Stenström, K., Prévôt, A. S. H.,
1042 Massoli, P., Canagaratna, M., Worsnop, D., and Decesari, S.: Primary and secondary biomass burning
1043 aerosols determined by proton nuclear magnetic resonance (¹H-NMR)
1044 spectroscopy during the 2008 EUCAARI campaign in the Po Valley (Italy), *Atmospheric Chemistry and
1045 Physics*, 14, 5089-5110, 10.5194/acp-14-5089-2014, 2014.

1046 Paglione, M., Gilardoni, S., Rinaldi, M., Decesari, S., Zanca, N., Sandrini, S., Giulianelli, L., Bacco, D.,
1047 Ferrari, S., Poluzzi, V., Scotto, F., Trentini, A., Poulain, L., Herrmann, H., Wiedensohler, A., Canonaco,
1048 F., Prévôt, A. S. H., Massoli, P., Carbone, C., Facchini, M. C., and Fuzzi, S.: The impact of biomass
1049 burning and aqueous-phase processing on air quality: a multi-year source apportionment study in
1050 the Po Valley, Italy, *Atmospheric Chemistry and Physics*, 20, 1233-1254, 10.5194/acp-20-1233-2020,
1051 2020.

1052 Passananti, M., Zapadinsky, E., Zanca, T., Kangasluoma, J., Mylly, N., Rissanen, M. P., Kurten, T., Ehn,
1053 M., Attoui, M., and Vehkamäki, H.: How well can we predict cluster fragmentation inside a mass
1054 spectrometer?, *Chem Commun (Camb)*, 55, 5946-5949, 10.1039/c9cc02896j, 2019.

1055 Peineke, C., Attoui, M. B., and Schmidt-Ott, A.: Using a glowing wire generator for production of
1056 charged, uniformly sized nanoparticles at high concentrations, *Journal of Aerosol Science*, 37, 1651-
1057 1661, 10.1016/j.jaerosci.2006.06.006, 2006.

1058 Peng, J. F., Hu, M., Wang, Z. B., Huang, X. F., Kumar, P., Wu, Z. J., Guo, S., Yue, D. L., Shang, D. J.,
1059 Zheng, Z., and He, L. Y.: Submicron aerosols at thirteen diversified sites in China: size distribution,
1060 new particle formation and corresponding contribution to cloud condensation nuclei production,
1061 *Atmos. Chem. Phys.*, 14, 10249-10265, 10.5194/acp-14-10249-2014, 2014.

1062 Rose, C., Sellegri, K., Velarde, F., Moreno, I., Ramonet, M., Weinhold, K., Krejci, R., Ginot, P.,
1063 Andrade, M., Wiedensohler, A., and Laj, P.: Frequent nucleation events at the high altitude station of
1064 Chacaltaya (5240 m a.s.l.), Bolivia, *Atmospheric Environment*, 102, 18-29,
1065 10.1016/j.atmosenv.2014.11.015, 2015.

1066 Saarikoski, S., Carbone, S., Decesari, S., Giulianelli, L., Angelini, F., Canagaratna, M., Ng, N. L.,
1067 Trimborn, A., Facchini, M. C., Fuzzi, S., Hillamo, R., and Worsnop, D.: Chemical characterization of
1068 springtime submicrometer aerosol in Po Valley, Italy, *Atmospheric Chemistry and Physics*, 12, 8401-
1069 8421, 10.5194/acp-12-8401-2012, 2012.

1070 Schobesberger, S., Junninen, H., Bianchi, F., Lonn, G., Ehn, M., Lehtipalo, K., Dommen, J., Ehrhart, S.,
1071 Ortega, I. K., Franchin, A., Nieminen, T., Riccobono, F., Hutterli, M., Duplissy, J., Almeida, J., Amorim,

1072 A., Breitenlechner, M., Downard, A. J., Dunne, E. M., Flagan, R. C., Kajos, M., Keskinen, H., Kirkby, J.,
1073 Kupc, A., Kurten, A., Kurten, T., Laaksonen, A., Mathot, S., Onnela, A., Praplan, A. P., Rondo, L.,
1074 Santos, F. D., Schallhart, S., Schnitzhofer, R., Sipila, M., Tome, A., Tsagkogeorgas, G., Vehkamäki, H.,
1075 Wimmer, D., Baltensperger, U., Carslaw, K. S., Curtius, J., Hansel, A., Petaja, T., Kulmala, M.,
1076 Donahue, N. M., and Worsnop, D. R.: Molecular understanding of atmospheric particle formation
1077 from sulfuric acid and large oxidized organic molecules, *Proc Natl Acad Sci U S A*, **110**, 17223-17228,
1078 10.1073/pnas.1306973110, 2013.

1079 Schraufnagel, D. E.: The health effects of ultrafine particles, *Exp Mol Med*, **52**, 311-317,
1080 10.1038/s12276-020-0403-3, 2020.

1081 Sebastian, M., Kompalli, S. K., Kumar, V. A., Jose, S., Babu, S. S., Pandithurai, G., Singh, S., Hooda, R.
1082 K., Soni, V. K., Pierce, J. R., Vakkari, V., Asmi, E., Westervelt, D. M., Hyvärinen, A.-P., and Kanawade,
1083 V. P.: Observations of particle number size distributions and new particle formation in six Indian
1084 locations, *Atmospheric Chemistry and Physics*, **22**, 4491-4508, 10.5194/acp-22-4491-2022, 2022.

1085 Shen, J., Bigi, A., Marinoni, A., Lampilahti, J., Kontkanen, J., Ciarelli, G., Putaud, J. P., Nieminen, T.,
1086 Kulmala, M., Lehtipalo, K., and Bianchi, F.: Emerging Investigator Series: COVID-19 lockdown effects
1087 on aerosol particle size distributions in northern Italy, *Environ Sci Atmos*, **1**, 214-227,
1088 10.1039/d1ea00016k, 2021.

1089 Shen, X. J., Sun, J. Y., Zhang, Y. M., Wehner, B., Nowak, A., Tuch, T., Zhang, X. C., Wang, T. T., Zhou, H.
1090 G., Zhang, X. L., Dong, F., Birmili, W., and Wiedensohler, A.: First long-term study of particle number
1091 size distributions and new particle formation events of regional aerosol in the North China Plain,
1092 *Atmospheric Chemistry and Physics*, **11**, 1565-1580, 10.5194/acp-11-1565-2011, 2011.

1093 Simon, M., Dada, L., Heinritzi, M., Scholz, W., Stolzenburg, D., Fischer, L., Wagner, A. C., Kürten, A.,
1094 Rörup, B., He, X.-C., Almeida, J., Baalbaki, R., Baccarini, A., Bauer, P. S., Beck, L., Bergen, A., Bianchi,
1095 F., Bräkling, S., Brilke, S., Caudillo, L., Chen, D., Chu, B., Dias, A., Draper, D. C., Duplissy, J., El-Haddad,
1096 I., Finkenzeller, H., Frege, C., Gonzalez-Carracedo, L., Gordon, H., Granzin, M., Hakala, J., Hofbauer,
1097 V., Hoyle, C. R., Kim, C., Kong, W., Lamkaddam, H., Lee, C. P., Lehtipalo, K., Leiminger, M., Mai, H.,
1098 Manninen, H. E., Marie, G., Marten, R., Mentler, B., Molteni, U., Nichman, L., Nie, W., Ojdanic, A.,
1099 Onnela, A., Partoll, E., Petäjä, T., Pfeifer, J., Philippov, M., Quéléver, L. L. J., Ranjithkumar, A.,
1100 Rissanen, M. P., Schallhart, S., Schobesberger, S., Schuchmann, S., Shen, J., Sipilä, M., Steiner, G.,
1101 Stozhkov, Y., Tauber, C., Tham, Y. J., Tomé, A. R., Vazquez-Pufleau, M., Vogel, A. L., Wagner, R.,
1102 Wang, M., Wang, D. S., Wang, Y., Weber, S. K., Wu, Y., Xiao, M., Yan, C., Ye, P., Ye, Q., Zauner-
1103 Wiecek, M., Zhou, X., Baltensperger, U., Dommen, J., Flagan, R. C., Hansel, A., Kulmala, M.,
1104 Volkamer, R., Winkler, P. M., Worsnop, D. R., Donahue, N. M., Kirkby, J., and Curtius, J.: Molecular
1105 understanding of new-particle formation from α -pinene between -50 and $+25$ °C,
1106 *Atmospheric Chemistry and Physics*, **20**, 9183-9207, 10.5194/acp-20-9183-2020, 2020.

1107 Sipilä, M., Sarnela, N., Jokinen, T., Henschel, H., Junninen, H., Kontkanen, J., Richters, S.,
1108 Kangasluoma, J., Franchin, A., Perakyla, O., Rissanen, M. P., Ehn, M., Vehkamäki, H., Kurten, T.,
1109 Berndt, T., Petaja, T., Worsnop, D., Ceburnis, D., Kerminen, V. M., Kulmala, M., and O'Dowd, C.:
1110 Molecular-scale evidence of aerosol particle formation via sequential addition of HIO₃, *Nature*, **537**,
1111 532-534, 10.1038/nature19314, 2016.

1112 Song, Z., Gao, W., Shen, H., Jin, Y., Zhang, C., Luo, H., Pan, L., Yao, B., Zhang, Y., Huo, J., Sun, Y., Yu,
1113 D., Chen, H., Chen, J., Duan, Y., Zhao, D., and Xu, J.: Roles of Regional Transport and Vertical Mixing
1114 in Aerosol Pollution in Shanghai Over the COVID-19 Lockdown Period Observed Above Urban
1115 Canopy, *Journal of Geophysical Research: Atmospheres*, **128**, e2023JD038540,
1116 <https://doi.org/10.1029/2023JD038540>, 2023.

1117 Stolzenburg, D., Fischer, L., Vogel, A. L., Heinritzi, M., Schervish, M., Simon, M., Wagner, A. C., Dada,
1118 L., Ahonen, L. R., Amorim, A., Baccarini, A., Bauer, P. S., Baumgartner, B., Bergen, A., Bianchi, F.,
1119 Breitenlechner, M., Brilke, S., Buenrostro Mazon, S., Chen, D., Dias, A., Draper, D. C., Duplissy, J., El
1120 Haddad, I., Finkenzeller, H., Frege, C., Fuchs, C., Garmash, O., Gordon, H., He, X., Helm, J., Hofbauer,
1121 V., Hoyle, C. R., Kim, C., Kirkby, J., Kontkanen, J., Kurten, A., Lampilahti, J., Lawler, M., Lehtipalo, K.,
1122 Leiminger, M., Mai, H., Mathot, S., Mentler, B., Molteni, U., Nie, W., Nieminen, T., Nowak, J. B.,

1123 Ojdanic, A., Onnela, A., Passananti, M., Petaja, T., Quelever, L. L. J., Rissanen, M. P., Sarnela, N.,
1124 Schallhart, S., Tauber, C., Tome, A., Wagner, R., Wang, M., Weitz, L., Wimmer, D., Xiao, M., Yan, C.,
1125 Ye, P., Zha, Q., Baltensperger, U., Curtius, J., Dommen, J., Flagan, R. C., Kulmala, M., Smith, J. N.,
1126 Worsnop, D. R., Hansel, A., Donahue, N. M., and Winkler, P. M.: Rapid growth of organic aerosol
1127 nanoparticles over a wide tropospheric temperature range, *Proc Natl Acad Sci U S A*, 115, 9122-
1128 9127, 10.1073/pnas.1807604115, 2018.

1129 Stolzenburg, D., Simon, M., Ranjithkumar, A., Kürten, A., Lehtipalo, K., Gordon, H., Ehrhart, S.,
1130 Finkenzeller, H., Pichelstorfer, L., Nieminen, T., He, X.-C., Brilke, S., Xiao, M., Amorim, A., Baalbaki, R.,
1131 Baccarini, A., Beck, L., Bräkling, S., Caudillo Murillo, L., Chen, D., Chu, B., Dada, L., Dias, A., Dommen,
1132 J., Duplissy, J., El Haddad, I., Fischer, L., Gonzalez Carracedo, L., Heinritzi, M., Kim, C., Koenig, T. K.,
1133 Kong, W., Lamkaddam, H., Lee, C. P., Leiminger, M., Li, Z., Makhmutov, V., Manninen, H. E., Marie,
1134 G., Marten, R., Müller, T., Nie, W., Partoll, E., Petäjä, T., Pfeifer, J., Philippov, M., Rissanen, M. P.,
1135 Rörup, B., Schobesberger, S., Schuchmann, S., Shen, J., Sipilä, M., Steiner, G., Stozhkov, Y., Tauber, C.,
1136 Tham, Y. J., Tomé, A., Vazquez-Pufleau, M., Wagner, A. C., Wang, M., Wang, Y., Weber, S. K.,
1137 Wimmer, D., Wlasits, P. J., Wu, Y., Ye, Q., Zauner-Wieczorek, M., Baltensperger, U., Carslaw, K. S.,
1138 Curtius, J., Donahue, N. M., Flagan, R. C., Hansel, A., Kulmala, M., Lelieveld, J., Volkamer, R., Kirkby,
1139 J., and Winkler, P. M.: Enhanced growth rate of atmospheric particles from sulfuric acid,
1140 *Atmospheric Chemistry and Physics*, 20, 7359-7372, 10.5194/acp-20-7359-2020, 2020.

1141 Ude, S. and de la Mora, J. F.: Molecular monodisperse mobility and mass standards from
1142 electrosprays of tetra-alkyl ammonium halides, *Journal of Aerosol Science*, 36, 1224-1237,
1143 <https://doi.org/10.1016/j.jaerosci.2005.02.009>, 2005.

1144 Vana, M., Komsaare, K., Hörrak, U., Mirme, S., Nieminen, T., Kontkanen, J., Manninen, H. E., Petäjä,
1145 T., Noe, S. M., and Kulmala, M.: Characteristics of new-particle formation at three SMEAR stations,
1146 *Boreal Environment Research*, 2016.

1147 Vanhanen, J., Mikkilä, J., Lehtipalo, K., Sipilä, M., Manninen, H. E., Siivola, E., Petäjä, T., and Kulmala,
1148 M.: Particle Size Magnifier for Nano-CN Detection, *Aerosol Science and Technology*, 45, 533-542,
1149 10.1080/02786826.2010.547889, 2011.

1150 Wang, Z., Wu, Z., Yue, D., Shang, D., Guo, S., Sun, J., Ding, A., Wang, L., Jiang, J., Guo, H., Gao, J.,
1151 Cheung, H. C., Morawska, L., Keywood, M., and Hu, M.: New particle formation in China: Current
1152 knowledge and further directions, *Science of The Total Environment*, 577, 258-266,
1153 10.1016/j.scitotenv.2016.10.177, 2017.

1154 Wang, Z. B., Hu, M., Pei, X. Y., Zhang, R. Y., Paasonen, P., Zheng, J., Yue, D. L., Wu, Z. J., Boy, M., and
1155 Wiedensohler, A.: Connection of organics to atmospheric new particle formation and growth at an
1156 urban site of Beijing, *Atmospheric Environment*, 103, 7-17, 10.1016/j.atmosenv.2014.11.069, 2015.

1157 Wang, Z. B., Hu, M., Sun, J. Y., Wu, Z. J., Yue, D. L., Shen, X. J., Zhang, Y. M., Pei, X. Y., Cheng, Y. F.,
1158 and Wiedensohler, A.: Characteristics of regional new particle formation in urban and regional
1159 background environments in the North China Plain, *Atmospheric Chemistry and Physics*, 13, 12495-
1160 12506, 10.5194/acp-13-12495-2013, 2013.

1161 Wu, Z., Hu, M., Yue, D., Wehner, B., and Wiedensohler, A.: Evolution of particle number size
1162 distribution in an urban atmosphere during episodes of heavy pollution and new particle formation,
1163 *Science China Earth Sciences*, 54, 1772-1778, 10.1007/s11430-011-4227-9, 2011.

1164 Wu, Z., Hu, M., Liu, S., Wehner, B., Bauer, S., Ma Bliing, A., Wiedensohler, A., Petäjä, T., Dal Maso, M.,
1165 and Kulmala, M.: New particle formation in Beijing, China: Statistical analysis of a 1-year data set,
1166 *Journal of Geophysical Research*, 112, 10.1029/2006jd007406, 2007.

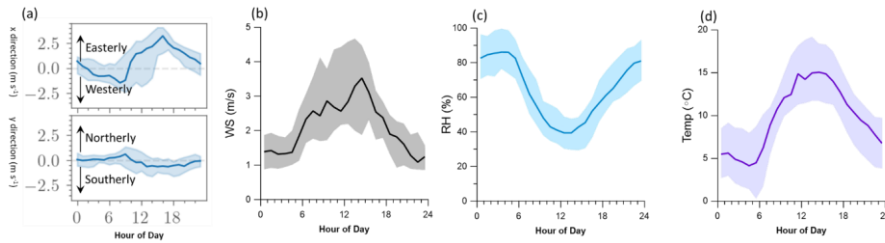
1167 Xiao, M., Hoyle, C. R., Dada, L., Stolzenburg, D., Kürten, A., Wang, M., Lamkaddam, H., Garmash, O.,
1168 Mentler, B., Molteni, U., Baccarini, A., Simon, M., He, X.-C., Lehtipalo, K., Ahonen, L. R., Baalbaki, R.,
1169 Bauer, P. S., Beck, L., Bell, D., Bianchi, F., Brilke, S., Chen, D., Chiu, R., Dias, A., Duplissy, J.,
1170 Finkenzeller, H., Gordon, H., Hofbauer, V., Kim, C., Koenig, T. K., Lampilahti, J., Lee, C. P., Li, Z., Mai,
1171 H., Makhmutov, V., Manninen, H. E., Marten, R., Mathot, S., Mauldin, R. L., Nie, W., Onnela, A.,
1172 Partoll, E., Petäjä, T., Pfeifer, J., Pospisilova, V., Quéléver, L. L. J., Rissanen, M., Schobesberger, S.,
1173 Schuchmann, S., Stozhkov, Y., Tauber, C., Tham, Y. J., Tomé, A., Vazquez-Pufleau, M., Wagner, A. C.,

1174 Wagner, R., Wang, Y., Weitz, L., Wimmer, D., Wu, Y., Yan, C., Ye, P., Ye, Q., Zha, Q., Zhou, X., Amorim,
1175 A., Carslaw, K., Curtius, J., Hansel, A., Volkamer, R., Winkler, P. M., Flagan, R. C., Kulmala, M.,
1176 Worsnop, D. R., Kirkby, J., Donahue, N. M., Baltensperger, U., El Haddad, I., and Dommen, J.: The
1177 driving factors of new particle formation and growth in the polluted boundary layer, *Atmospheric
1178 Chemistry and Physics*, 21, 14275-14291, 10.5194/acp-21-14275-2021, 2021.
1179 Xiao, S., Wang, M. Y., Yao, L., Kulmala, M., Zhou, B., Yang, X., Chen, J. M., Wang, D. F., Fu, Q. Y.,
1180 Worsnop, D. R., and Wang, L.: Strong atmospheric new particle formation in winter in urban
1181 Shanghai, China, *Atmospheric Chemistry and Physics*, 15, 1769-1781, 10.5194/acp-15-1769-2015,
1182 2015.
1183 Yan, C., Yin, R., Lu, Y., Dada, L., Yang, D., Fu, Y., Kontkanen, J., Deng, C., Garmash, O., Ruan, J.,
1184 Baalbaki, R., Schervish, M., Cai, R., Bloss, M., Chan, T., Chen, T., Chen, Q., Chen, X., Chen, Y., Chu, B.,
1185 Dällenbach, K., Foreback, B., He, X., Heikkinen, L., Jokinen, T., Junninen, H., Kangasluoma, J.,
1186 Kokkonen, T., Kurppa, M., Lehtipalo, K., Li, H., Li, H., Li, X., Liu, Y., Ma, Q., Paasonen, P., Rantala, P.,
1187 Pileci, R. E., Rusanen, A., Sarnela, N., Simonen, P., Wang, S., Wang, W., Wang, Y., Xue, M., Yang, G.,
1188 Yao, L., Zhou, Y., Kujansuu, J., Petäjä, T., Nie, W., Ma, Y., Ge, M., He, H., Donahue, N. M., Worsnop, D.
1189 R., Veli-Matti, K., Wang, L., Liu, Y., Zheng, J., Kulmala, M., Jiang, J., and Bianchi, F.: The Synergistic
1190 Role of Sulfuric Acid, Bases, and Oxidized Organics Governing New-Particle Formation in Beijing,
1191 *Geophysical Research Letters*, 48, 10.1029/2020gl091944, 2021.
1192 Yan, C., Nie, W., Vogel, A. L., Dada, L., Lehtipalo, K., Stolzenburg, D., Wagner, R., Rissanen, M. P.,
1193 Xiao, M., Ahonen, L., Fischer, L., Rose, C., Bianchi, F., Gordon, H., Simon, M., Heinritzi, M., Garmash,
1194 O., Roldin, P., Dias, A., Ye, P., Hofbauer, V., Amorim, A., Bauer, P. S., Bergen, A., Bernhammer, A.-K.,
1195 Breitenlechner, M., Brilke, S., Buchholz, A., Mazon, S. B., Canagaratna, M. R., Chen, X., Ding, A.,
1196 Dommen, J., Draper, D. C., Duplissy, J., Frege, C., Heyn, C., Guida, R., Hakala, J., Heikkinen, L., Hoyle,
1197 C. R., Jokinen, T., Kangasluoma, J., Kirkby, J., Kontkanen, J., Kürten, A., Lawler, M. J., Mai, H., Mathot,
1198 S., Mauldin, R. L., Molteni, U., Nichman, L., Nieminen, T., Nowak, J., Ojdanic, A., Onnela, A., Pajunoja,
1199 A., Petäjä, T., Piel, F., Quéléver, L. L. J., Sarnela, N., Schallhart, S., Sengupta, K., Sipilä, M., Tomé, A.,
1200 Tröstl, J., Väisänen, O., Wagner, A. C., Ylisirniö, A., Zha, Q., Baltensperger, U., Carslaw, K. S., Curtius,
1201 J., Flagan, R. C., Hansel, A., Riipinen, I., Smith, J. N., Virtanen, A., Winkler, P. M., Donahue, N. M.,
1202 Kerminen, V.-M., Kulmala, M., Ehn, M., and Worsnop, D. R.: Size-dependent influence of
1203 NO_x on the growth rates of organic aerosol particles, *Science Advances*, 6, eaay4945,
1204 doi:10.1126/sciadv.aay4945, 2020.
1205 Yao, L., Wang, M.-Y., Wang, X.-K., Liu, Y.-J., Chen, H.-F., Zheng, J., Nie, W., Ding, A.-J., Geng, F.-H.,
1206 Wang, D.-F., Chen, J.-M., Worsnop, D. R., and Wang, L.: Detection of atmospheric gaseous amines
1207 and amides by a high-resolution time-of-flight chemical ionization mass spectrometer with
1208 protonated ethanol reagent ions, *Atmospheric Chemistry and Physics*, 16, 14527-14543,
1209 10.5194/acp-16-14527-2016, 2016.
1210 Yao, L., Garmash, O., Bianchi, F., Zheng, J., Yan, C., Kontkanen, J., Junninen, H., Mazon, S. B., Ehn, M.,
1211 Paasonen, P., Sipilä, M., Wang, M. Y., Wang, X. K., Xiao, S., Chen, H. F., Lu, Y. Q., Zhang, B. W., Wang,
1212 D. F., Fu, Q. Y., Geng, F. H., Li, L., Wang, H. L., Qiao, L. P., Yang, X., Chen, J. M., Kerminen, V. M.,
1213 Petaja, T., Worsnop, D. R., Kulmala, M., and Wang, L.: Atmospheric new particle formation from
1214 sulfuric acid and amines in a Chinese megacity, *Science*, 361, 278+, 10.1126/science.aao4839, 2018.
1215 Yu, H., Zhou, L., Dai, L., Shen, W., Dai, W., Zheng, J., Ma, Y., and Chen, M.: Nucleation and growth of
1216 sub-3 nm particles in the polluted urban atmosphere of a megacity in China, *Atmospheric Chemistry
1217 and Physics*, 16, 2641-2657, 10.5194/acp-16-2641-2016, 2016.
1218 Yue, D. L., Hu, M., Wang, Z. B., Wen, M. T., Guo, S., Zhong, L. J., Wiedensohler, A., and Zhang, Y. H.:
1219 Comparison of particle number size distributions and new particle formation between the urban and
1220 rural sites in the PRD region, China, *Atmospheric Environment*, 76, 181-188,
1221 10.1016/j.atmosenv.2012.11.018, 2013.
1222 Zha, Q., Huang, W., Aliaga, D., Peräkylä, O., Heikkinen, L., Koenig, A. M., Wu, C., Enroth, J., Gramlich,
1223 Y., Cai, J., Carbone, S., Hansel, A., Petäjä, T., Kulmala, M., Worsnop, D., Sinclair, V., Krejci, R.,
1224 Andrade, M., Mohr, C., and Bianchi, F.: Measurement report: Molecular-level investigation of

1225 atmospheric cluster ions at the tropical high-altitude research station Chacaltaya (5240 m a.s.l.) in
1226 the Bolivian Andes, *Atmospheric Chemistry and Physics*, 23, 4559-4576, 10.5194/acp-23-4559-2023,
1227 2023.
1228 Zha, Q., Yan, C., Junninen, H., Riva, M., Sarnela, N., Aalto, J., Quéléver, L., Schallhart, S., Dada, L.,
1229 Heikkinen, L., Peräkylä, O., Zou, J., Rose, C., Wang, Y., Mammarella, I., Katul, G., Vesala, T., Worsnop,
1230 D. R., Kulmala, M., Petäjä, T., Bianchi, F., and Ehn, M.: Vertical characterization of highly oxygenated
1231 molecules (HOMs) below and above a boreal forest canopy, *Atmospheric Chemistry and Physics*, 18,
1232 17437-17450, 10.5194/acp-18-17437-2018, 2018.
1233 Zheng, Y., Chen, Q., Cheng, X., Mohr, C., Cai, J., Huang, W., Shrivastava, M., Ye, P., Fu, P., Shi, X., Ge,
1234 Y., Liao, K., Miao, R., Qiu, X., Koenig, T. K., and Chen, S.: Precursors and Pathways Leading to
1235 Enhanced Secondary Organic Aerosol Formation during Severe Haze Episodes, *Environ Sci Technol*,
1236 55, 15680-15693, 10.1021/acs.est.1c04255, 2021.

1237

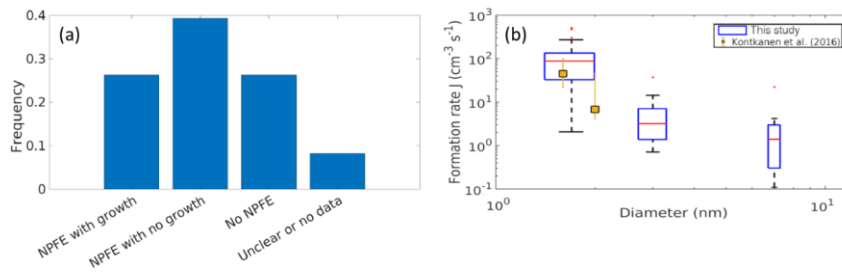
1238



1239

1240 **Figure 1.** The diurnal variations of (a) average wind vectors, (b) wind speed, (c) relative humidity (RH), and (d)
1241 temperature.

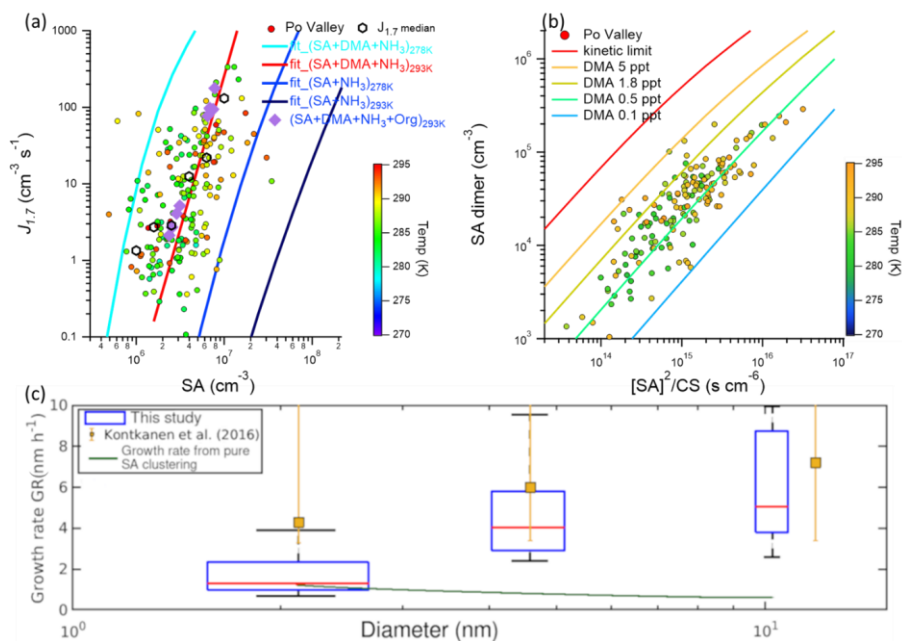
1242



1243

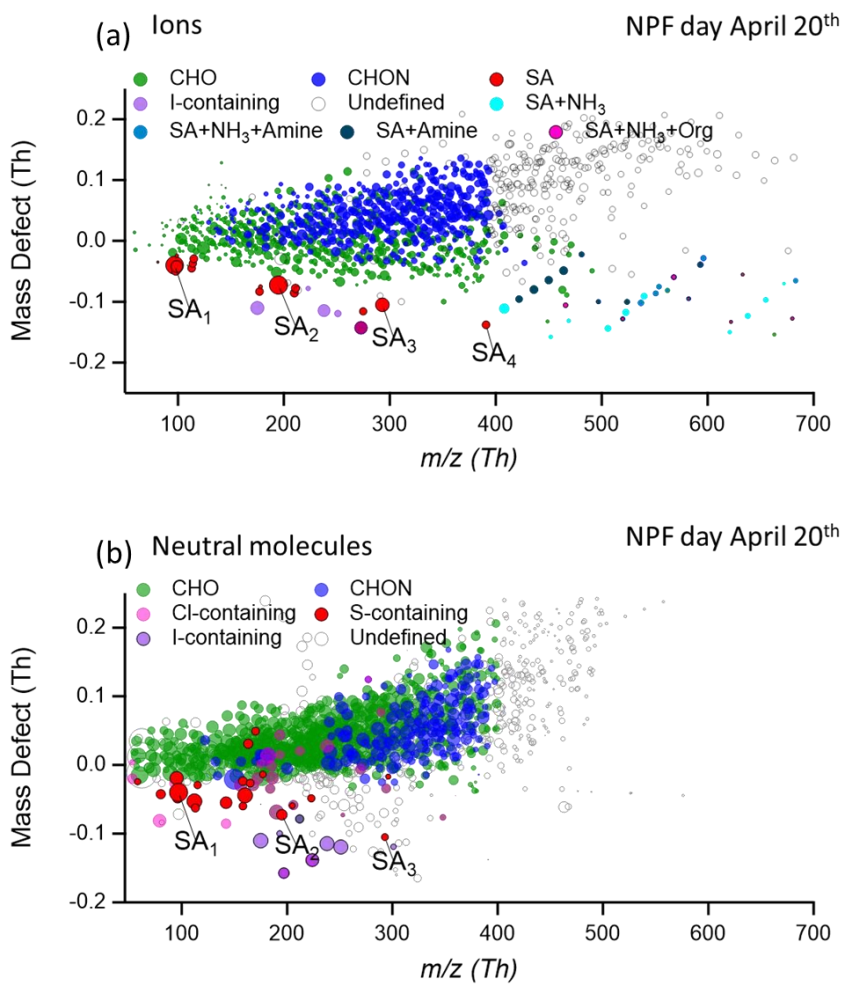
1244 **Figure 2.** (a) The frequency of NPF events with and without growth, of days without NPF,
1245 unclear classification or no data during this study, (b) calculated formation rates at 1.7 nm, 3 nm and 7 nm from this
1246 study and values reported by Kontkanen et al. 2016 (yellow squares). The red lines are the median values of the
1247 maximum formation rates measured during an NPF event, the blue boxes show the values between 25th and 75th
1248 percentiles and the black whiskers mark the 5th and 95th percentiles. Red dots are outliers, and the width of the
1249 box is proportional to the square root of the number of the J values.

1250



1251

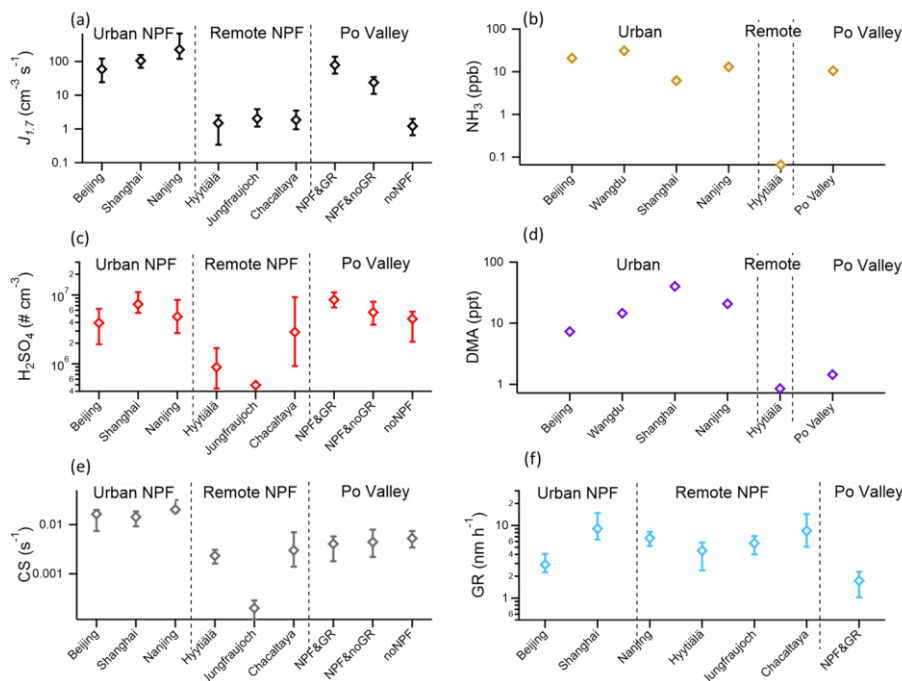
1252 **Figure 3.** (a) The formation rate of 1.7 nm particles ($J_{1.7}$) versus SA concentrations in during springtime in the Po
 1253 Valley (shown as circles) and experimental results from CLOUD chamber experiments (shown as solid diamonds).
 1254 The solid lines are from fitted results of CLOUD chamber experiments and the black hexagon represented the
 1255 mean values under different SA levels, (b) the relationship between sulfuric acid dimer concentration (SA dimer),
 1256 the square of monomer concentrations (SA)², and the CS. The lines are from the kinetic model simulations under
 1257 different DMA levels and the dots are from the measurement. In (a) and (b), the results from the field
 1258 measurements are from the daytime (10:00 – 14:00 LT) and color-coded by the temperature at the site. The $J_{1.7}$
 1259 and corresponding SA concentrations of CLOUD chamber results are from previous literature (Xiao et al., 2021).
 1260 (c) Calculated growth rates for 1.5 – 3 nm, 3 – 7 nm, and 7 – 15 nm from this study and values reported by
 1261 Kontkanen et al. (2016, yellow squares). The red horizontal lines are the median values, the blue boxes show the
 1262 values between 25th and 75th percentiles and the black whiskers mark the 5th and 95th percentiles. The green solid
 1263 line represents predicted growth rates from pure sulfuric acid without organics condensation (Stolzenburg et al.,
 1264 2020). The width of the box is proportional to the square root of the number of the GR values.



1265

1266 **Figure 4.** Mass defect plots, which represent the difference between compounds' exact mass and nominal mass,
 1267 for (a) ion clusters and (b) neutral clusters during the NPF period (10:00 – 14:00 LT) of April 20. The size of the
 1268 dots is proportional to the logarithm of the signal intensity of each cluster.

1269



1270

1271 **Figure 5.** Parameters and gaseous precursors of NPF in the Po Valley and other environments. (a) formation rate
 1272 of sub-2 nm particles, (b) the atmospheric NH_3 concentrations, (c) SA concentrations, (d) DMA concentrations,
 1273 (e) CS levels, and (f) growth rate in different environments. The diamond dots represent the median values, and
 1274 the error bars represent the 25th and 75th percentiles. For the Po Valley data, the formation rates, growth rates, SA
 1275 concentrations and CS data were selected for 10:00 – 14:00 LT. The formation rates, growth rates, SA
 1276 concentrations and CS during NPF in Beijing, Shanghai, Hyytiälä, Jungfraujoch and Chacaltaya are from Deng
 1277 et al. (2020). The GR calculation range varies for different sites. Beijing (GR_{7-15} , (Deng et al., 2020)), Shanghai
 1278 (GR_{7-25} , (Yao et al., 2018)), Nanjing (GR_{3-20} , (Yu et al., 2016)), Hyytiälä (GR_{3-20} , (Vana et al., 2016)),
 1279 Jungfraujoch (GR_{7-20} , (Boulon et al., 2010)), Chacaltaya (GR_{7-20} , (Rose et al., 2015)), and Po Valley (GR_{7-15} , this
 1280 study) are used for comparison. The NH_3 and DMA concentrations are from literature, which is listed in the Table
 1281 S1. Half of the limit of detection (LOD) of DMA concentrations in Hyytiälä was applied in panel d. DMA
 1282 concentrations in Po Valley was not presented since it is not quantified in this study.